PROBE STUDIES OF PLASMA IN A MAGNETIC WELL

by

D. A. BOYD

June, 1967

Thesis presented in part
fulfilment of the requirements
for the Degree of
Master of Science in Physics
at the
University of Cape Town

CONTENTS

ABSTRACT

A modified theta pinch device proposed by Andreoletti has been investigated. Magnetic field measurements have revealed that the device produces a magnetic well with mirror ratio 1.06. Further magnetic probe measurements have enabled fairly detailed description of the plasma dynamics in the central horizontal plane to be given. A method developed by Lovberg in which the magnetic measurements are coupled with measurements with a double floating electric probe, was used to measure the electron density in certain favourable circumstances.

SECTION 1

INTRODUCTION

1. INTRODUCTION

The study of magnetic geometries in which the field strength increases towards the periphery of the system, has intensified as plasma physicists concluded that these devices should be able to ensure a hydromagnetically stable plasma. Certainly the early interest in the Cusp Geometry was encouraged by the promise of stability which would follow because the field strength did increase outwards.

The devices which provide the above criterion may be divided into two braod classes. One, the $\beta = 1$ variety in which the magnetic field is totally excluded from the plasma; and two, the adiabatic traps, the true minimum-B, in which there is a substantial magnetic field within the plasma. $\beta = \frac{nkT}{B^2/2\mu_0}$ In both categories the essential condition is that the magnetic field lines must be convex towards the plasma. It is not possible to satisfy this criterion in any but an open ended device (3). There is one exception to this, that is the Astron Concept. To quote Christofilos (4) "... it is impossible to establish

with vacuum fields a continuous minimum-B configuration and thus provide hydromagnetic stability free of 'ballooning' or 'resistive' modes. The reasoning is simple. A continuous minimum-B configuration requires that the confining field increases radially. Such a monotonic increase towards the radial direction implies, that, in curl-free fields, the field intensity must increase monotonically. Thus, the field pattern cannot be closed. If the field is not curl-free however, such as the field resulting from placing relativistic electron coils in the plasma, it is possible to achieve a monotonic increase along the field lines." In other closed-ended systems one can only achieve a sort of average minimum-B with $\frac{\partial^2 V}{\partial \phi^2} < 0$ (5) where V is the volume enclosed by a magnetic surface and ϕ is the flux that is enclosed.

In the $\beta = 1$ class the Cusp is the only representative. Cusps are poor adiabatic containers (6) and so they are generally operated with $\beta = 1$ (7). Unfortunately they leak badly through the

the line and point cusps because the space charge fields at plasma-magnetic field interface necessary to keep the leaks small are shorted out by cold background plasma. In the Cusp configuration the plasma is stable against interchanges.

A great deal of work has been done experimentally and theoretically with adiabatic minimum-B traps. The concept of combining crossed magnetic fields to create a system both hydromagnetically stable and capable of adiabatic containment was put forward by Berkowitz et al (8) in 1958. The first experimental verification of the stabilization offered by this approach, was achieved by M.S. Ioffe (9) in 1961. Since then a great deal of work has been done on the concept. Taylor and Hastie (10) have shown that the configurations are stable even at finite β and others have extended the theory to include many types of instability (11). Several experiments are being run in this geometry, both with Ioffe bars (12) and in a new system where the magnetic field is formed by a coil in the shape of the seam on a tennis ball (13).

These systems are stable against interchanges and the confinement time is usually increased by a factor of 5 or more. Most of the devices appear to be troubled by micro-instabilities (14).

Recently Grad (15) has been severely criticizing the theoretical foundation of the minimum-B concept, but nevertheless experimentally minimum-B geometries are more stable than other kinds of magnetic geometry.

We have been studying a device proposed by J. Andreoletti (16) in 1964. It is a modified theta-pinch device which consists of two truncated tetrahedra joined when they have a square cross-section (see fig. 2(a)). Our magnetic measurements have shown that the device produces a magnetic well with a mirror ratio of 1.06.

This device could be operated in either of the two modes described above. In the $\beta = 1$ mode, a highly ionized blob of plasma could be injected and then compressed by the external field. Certainly the field lines would be gravely

distorted and the minimum-B property might be destroyed. However the device should have advantages over the cusp geometry, because it will leak less. Long theta pinches also work in this mode, but they leak badly along the magnetic axis. This device, the Tetrahedral Spire, has advantages in this sphere as well. It has strong mirrors along the central axis (mirror ratio = 2) which will help to inhibit these losses.

It would be more difficult to operate the device as an adiabatic trap, because any low frequency magnetic field would suffer severe flux lossed through the walls of the spire. These flux losses we have found do reduce the well depth substantially. With a D.C. current, the well all but disappears. These facts make reasonably high frequency operation a necessity. It might be possible to establish a relatively diffuse low β plasma in the device and then crowbar the external circuit so that the external current decays over a period of the order of 100 μseconds, and so test the spire as an adiabatic trap.

Unfortunately we have not been able to operate the spire in either of these two modes. We could neither crowbar the circuit nor inject the plasma. It was necessary to rely on the external electric field at current zeroes to ionize the gas. This prevented any real test of the spire as a minimum-B device.

We have used magnetic probes to study the plasma dynamics in the central horizontal plane of the spire and a technique of floating double electric probes developed by Lovberg (1) to measure the electron density. From these measurements we have been able to reconstruct a time resolved picture of the dynamics of the current sheath, the changes in magnetic pressure and the changes in electron density during the discharge.

SECTION 2

THE SPIRE &

VACUUM CHAMBER

2.1 THE SPIRE

The spire consists of two truncated rectangular tetrahedra which are joined when each has a square cross-section. See fig. 2(a). It was made in two sections which could be bolted together by four bolts through two connecting bars. The sides of the spire were made from 1/16" copper sheet and the connecting bars were of brass with cross-section of $\frac{1}{4}$" x $\frac{1}{2}$". The complete spire could be bolted to the tab plates of the rest of the circuit through another pair of connecting bars. A strip of soft lead was used to line this gap to ensure good electrical contact.

Spire dimensions

The dimensions of the centre cross-section:	12cm x 12cm
The dimensions of the end sections:	3cm x 30cm
The length along the z-axis:	24cm

fig 2(a) The Tetrahedral Spire shown with connecting bars but without bolts

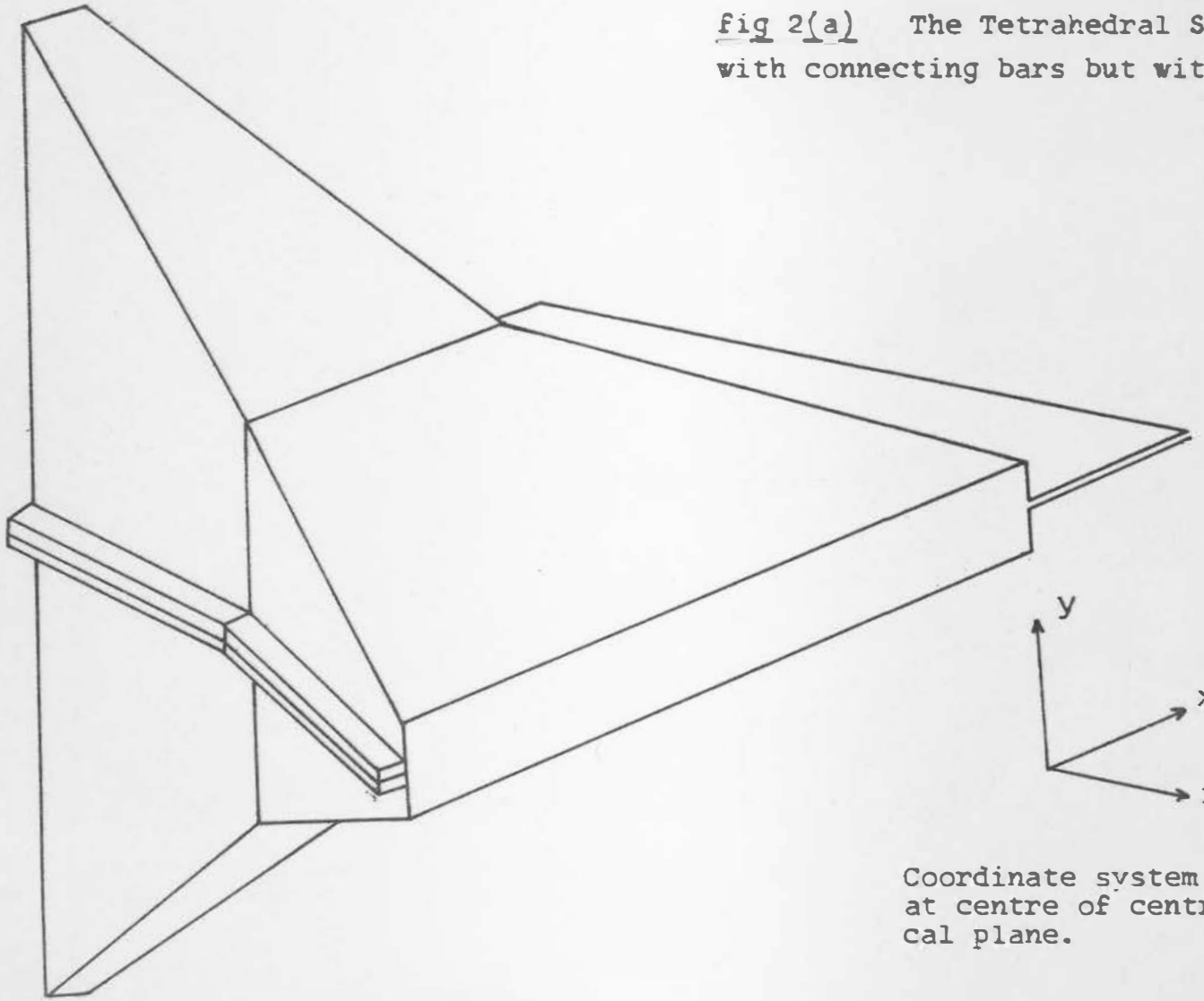

Coordinate system with origin at centre of central vertical plane.

THE VACUUM CHAMBER AND PUMPING SYSTEM

Early attempts at making a vacuum chamber which closely fitted the walls of the spire proved abortive. It was then decided to build a chamber which fitted only to the walls with the smaller slope. See the diagram in fig. 2(b). This model did away with the very awkward discontinuity in slope at the centre. The sides of the chamber were made of $\frac{1}{4}$" perspex sheet. The end pieces were $\frac{1}{2}$" thick. In one end-piece, a vacuum system connection was provided. There were 5 ports in the opposite end-piece; one at the centre and four more spaced at $1\frac{1}{2}$ cm from each other to allow access for the probes into the central horizontal plane.

The vacuum system consisted of an oil diffusion pump backed by a rotary pump and the pressure was monitored with a Pirani guage. This Pirani guage was calibrated with a McCleod guage.

The chamber was filled to the initial pressure with air by allowing atmospheric air to leak in slowly through a valve. By adjusting the pumping speed it was possible to set up a dynamic equilibrium with the gas pressure at 20 microns Hg.

fig. 2(b) The Vacuum Chamber

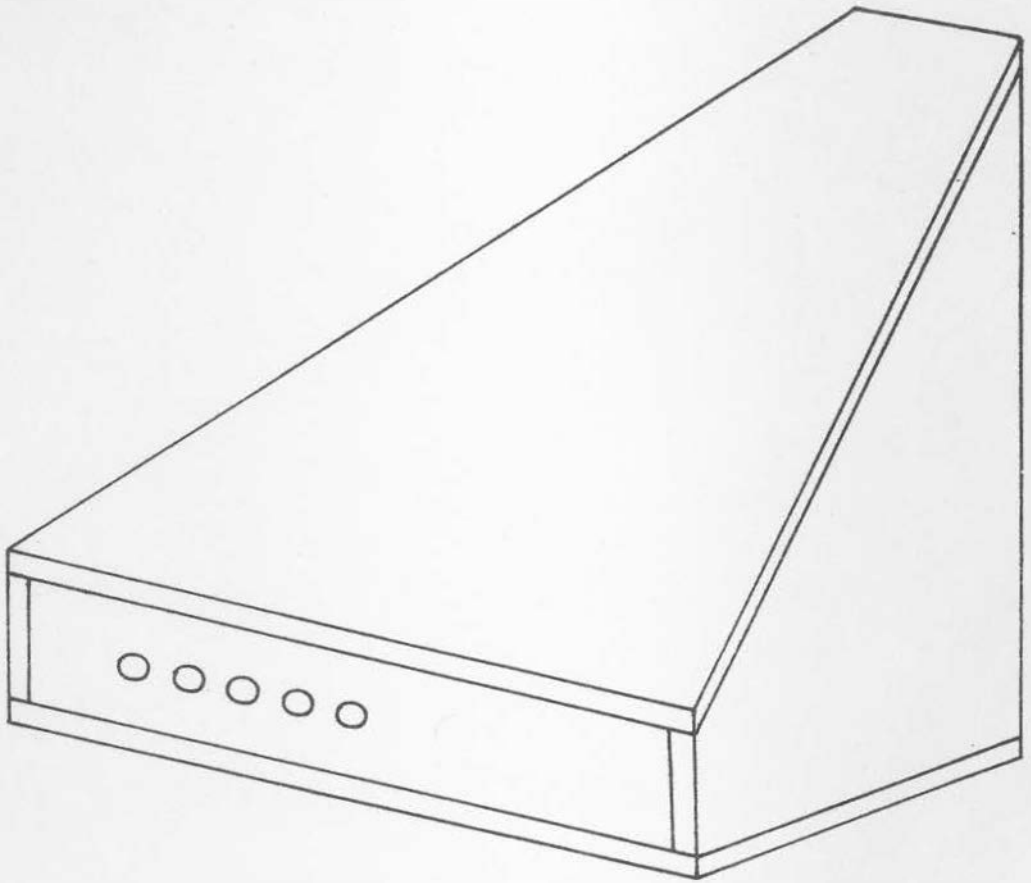

5 cm

SECTION 3

OUTLINE OF EXPERIMENTS

EXPERIMENTAL METHOD

3.1 The experimental program fell naturally into three parts. First it was necessary to see if the device did indeed produce a magnetic well. To demonstrate this a set of vacuum magnetic field measurements was made to map the extent and shape of the well. A second set of magnetic field measurements was made with a plasma in the device. These measurements enabled the position of the current sheath in the central horizontal plane to be found as a function of time during the discharge and a set of magnetic pressure maps to be drawn. Thirdly a set of electrical measurements was made. This consisted of measuring the z-component of the electric field in the central horizontal plane. The results when coupled with the results of the magnetic measurements made it possible to calculate the electron density in certain favourable circumstances.

The general experimental set-up for the three sets of measurements will be sketched below. Further descriptions will be given when each set of measurements is discussed in detail.

VACUUM FIELD MEASUREMENTS

3.2 The spire was connected to a very low energy discharge circuit. The probe used to measure the magnetic field consisted of three mutually perpendicular coils of approximately 200 turns each, wound on bobbins with radius of 1 mm. A system operating in a cylindrical geometry was used to position the probe inside the spire. The output of the coils was fed directly into a double beam oscilloscope. A double pole switch was used to switch in the input of two of the component coils alternately, as only two components could be recorded at one time. The traces of the pairs of components were photographed and later measured.

fig. 3(a) Experimental Layout to Measure Vacuum Magnetic Field

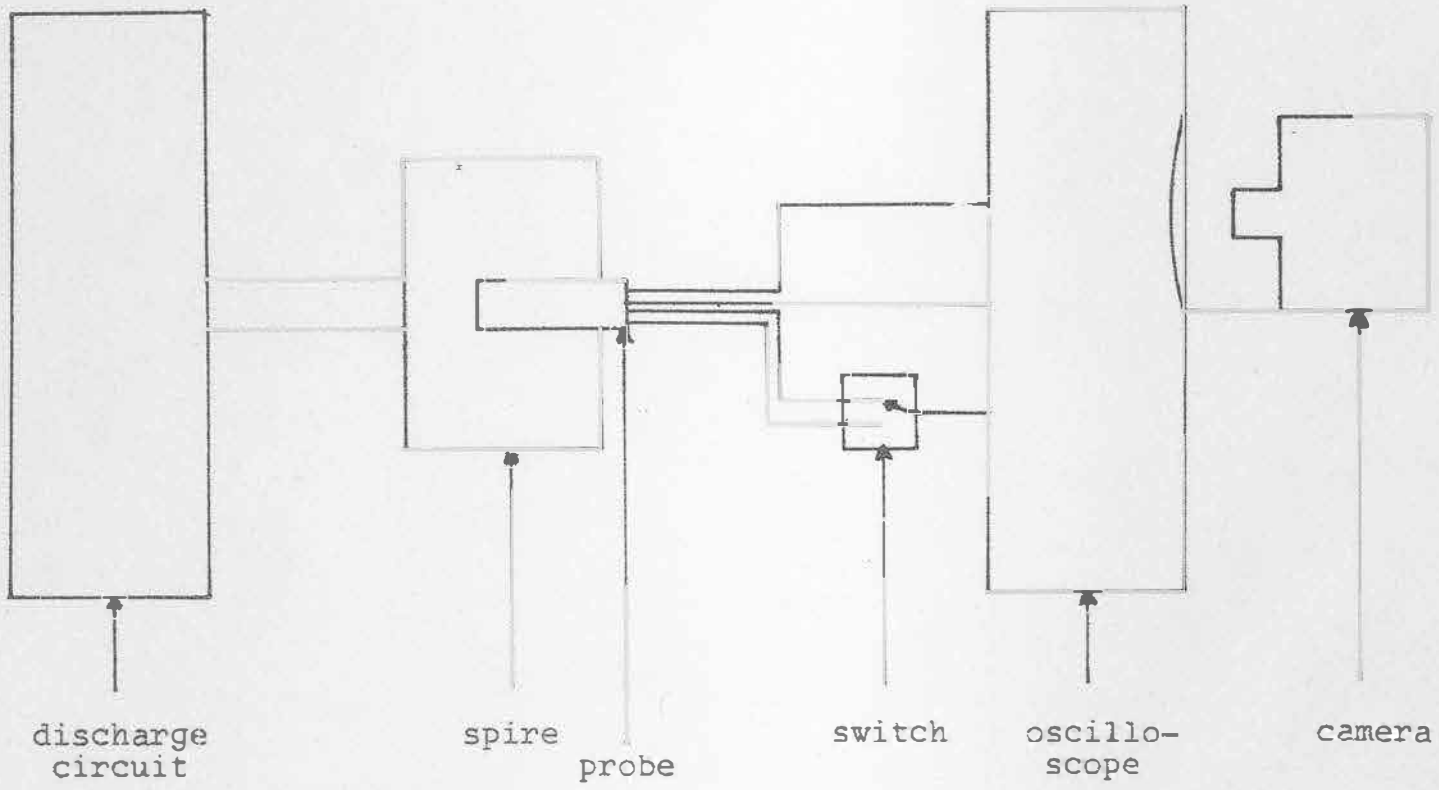

MAGNETIC FIELD MEASUREMENTS WITH PLASMA

3.3 For these experiments with a plasma in the device, the spire was connected to a relatively low energy (one Kilojoule) condenser bank. The measurements were confined to the central horizontal plane (Y = 0). The probe consisted of three mutually perpendicular coils of approximately 25 turns each, wound on bobbins with a radius of 1 mm. The probe was enclosed in a glass tube with an outer diameter of 4.5 mm. On each traverse line the glass tube was pushed in until it touched the far wall of the vacuum chamber. Then the probe was positioned in the appropriate place inside the tube. The output of the coils was fed into coaxial cables and from these into the integrating circuits. The output of the integrators was fed into a double beam oscilloscope where the traces were photographed. A small coil fitted between the tab plates of the spire acted as a current monitor. Switches on the integrators enabled the following pairs of traces to be photographed alternately B_z, I and B_x, B_y.

fig. 3(b) Experimental Layout for Magnetic Measurements with Plasma Present

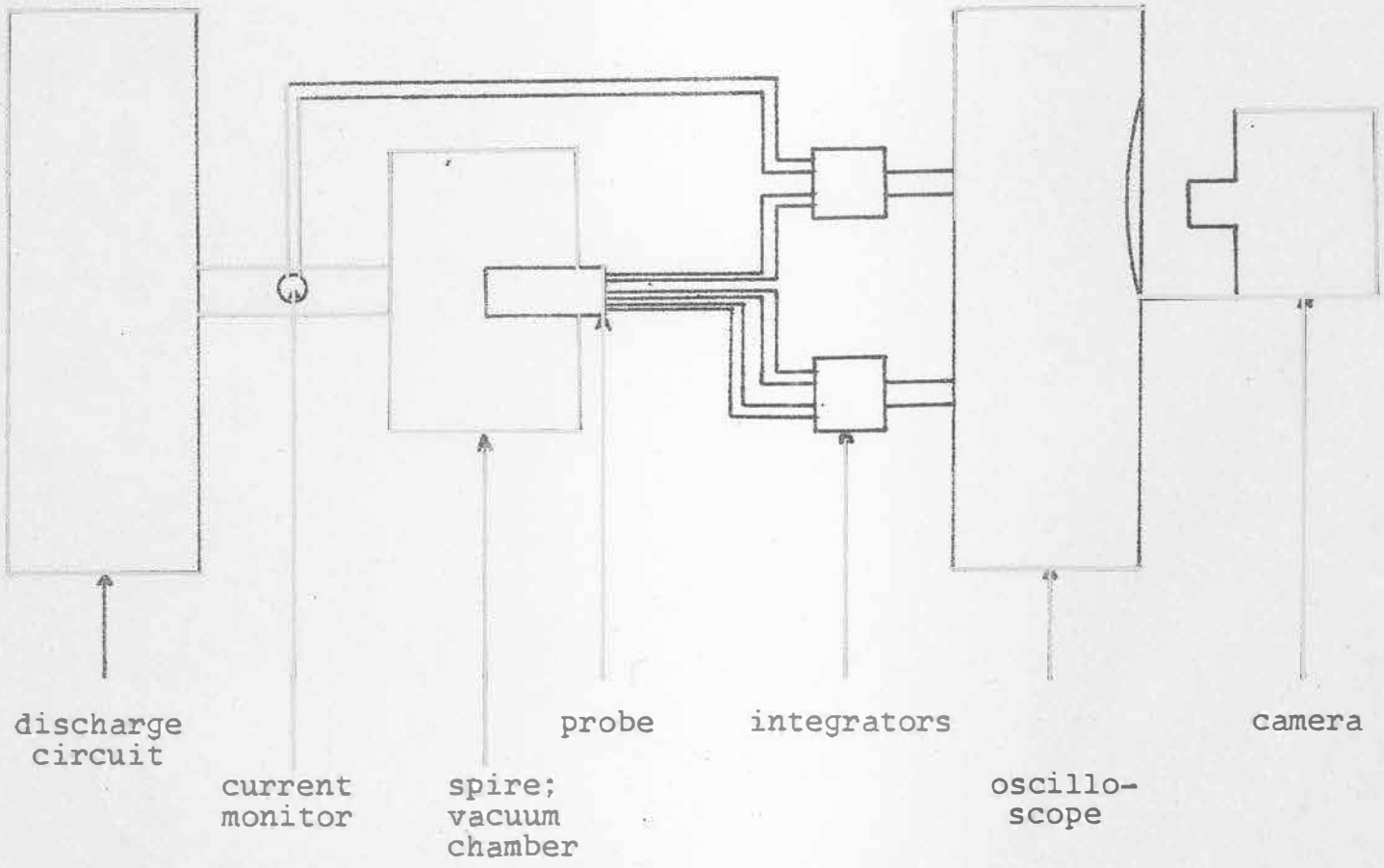

ELECTRIC FIELD MEASUREMENTS

3.4 For these measurements the spire remained connected to the Kilojoule capacitor bank. The E_z component of the electric field in the central horizontal plane was measured with a double floating probe. The output of the probe was fed into a very high impedence voltage divider and then one tenth of this output voltage was fed by coaxial cable into a pulse transformer which isolated the probe circuit and plasma from earth. From the pulse transformer the signal went directly into a double beam oscilloscope, where the trace was photographed. Each electric probe signal was photographed with the signal from the current monitor on the other beam of the oscilloscope.

fig 3(c) The Experimental Layout for the Electric Field Measurements

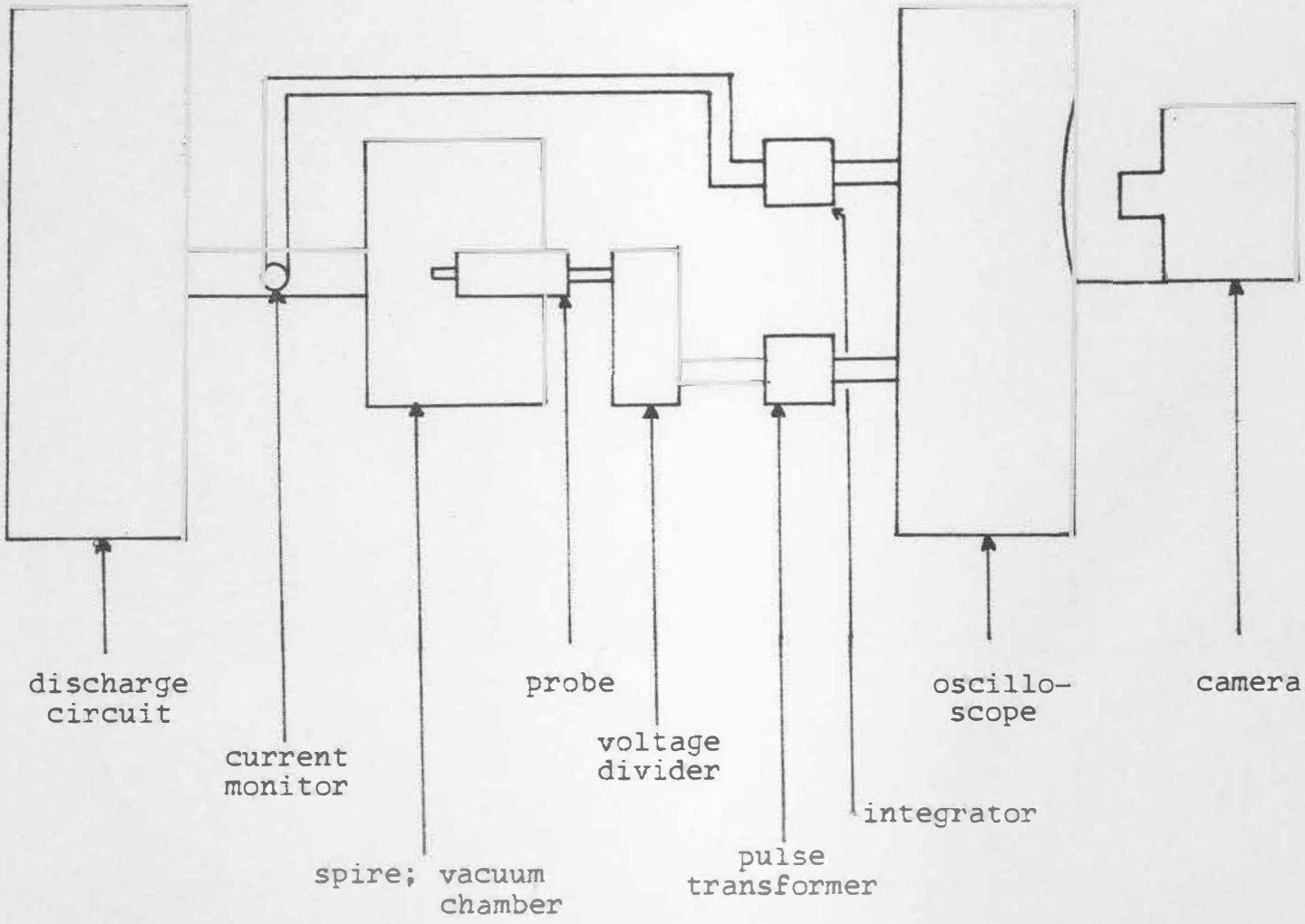

SECTION 4

THE VACUUM MAGNETIC FIELD

4. THE MEASUREMENT OF THE VACUUM MAGNETIC FIELD

4.1 The experimental layout for this set of measurements can be seen in fig. 3(a). The discharge circuit used is displayed in fig. 4(a). For these measurements the ringing frequency of the circuit was about 2.5×10^4 Hz. The skin depth $\delta = \sqrt{\frac{2}{\mu\omega\sigma}}$ at this frequency is about 0.4 mm. As the walls of the spire are 1.6 mm thick this ensures that very little flux leaks through the walls.

A magnetic probe unit was used to map the field inside the spire. This unit consisted of three mutually perpendicular coils of 46 SWG enamel covered copper wire. Each coil had four layers of approximately 50 turns each wound on a polyethelene bobbin of radius 1 millimeter. The probe was not electrostatically shielded. Fig. 4(c) shows diagrams of the probe unit and the bobbin. The signals of the coils were normalized relative to each other by placing them at the centre of a small Helmholtz coil and comparing their outputs. The following normalization constants were found.

Coil	Normalization Constant
R	1.00
X	0.94
O	1.01

The probe unit was positioned at a set of lattice points on the planes, and within the octant, shown in Fig. 4(d). The step lengths between lattice points was $1\frac{1}{2}$ cm for the R coordinate and X coordinate. Measurements were taken with the θ coordinate values of 0°, 10°, $17\frac{1}{2}^{\circ}$, 25°. In fig. 4(d) the positioning mechanism used can be seen. The R coordinate was measured from the pivot point of the probe unit at the mouth of the spire. The X axis was parallel to the mouth of the spire with its zero at the midpoint of the mouth. A measure of the rotation of the probe about the x-axis was given by the θ coordinate. Clockwise rotations were considered positive.

Signals from the probe were displayed on a Tektronix 551 double-beam oscilloscope and photographed. For each probe position two photographs were taken, one of the R and X signals, and one of the R and θ signals. The voltage

signals from the coils are proportioned to the rate of change of $\underline{B}$, and were recorded directly, without integration. This was advisable to avoid introducing different attenuations, by the two or more integrating circuits required. Since the current in the spire has a time dependence of $e^{-\alpha t} \sin \omega t$ the output voltage signals have the dependence $e^{-\alpha t} \cos(\omega t + \delta)$ where δ is very small. The initial peaks of such traces are usually noisy, so in all cases the amplitude of the second peak ($t = \tau/2 = \pi/\omega$) was measured. In this way three orthogonal components of the field were recorded. After taking the mean of the two R component values, the value of the magnetic field B was calculated in arbitrary units and then normalised so that the value of the field strength at the origin was 100.

Some of the results of these measurements are displayed in figs. 4(e), 4(f) and 4(g). They reveal a well with an increase of 6% in field strength at the boundary compared with the field strength at the centre i.e. a mirror ratio of 1.06.

A formula for the field

Dr H.S.T. Driver made an attempt to calculate the magnetic field of the spire. The basic assumption was that the current had no Z-component i.e. that the current was parallel to the central vertical plane everywhere. This enabled one to divide the spire up into a set of elemental strips and then to calculate the field using the University computer, by summing the contribution of each strip over all strips. Typically the number of strips used was 50 as it was found that no increase in accuracy was obtained by using more than this. At first uniform direct currents were assumed and later in an attempt to approximate to oscillatory conditions, the current still without any Z-component was assumed to increase linearly with Z.

All these approaches did not produce even a poor approximation to the form and strength of the field found from measurements. It was concluded that the assumption that the current has no Z-component is unjustified and that the form of the field obtained depends on the current

distribution departing radically from the no Z-component criterion.

To calculate the variation of inductance within the spire, which in turn would regulate the current distribution, it is necessary to know the current paths. Unfortunately to find these current paths was the reason for attempting to calculate the inductance. So faced with this vicious circle, all attempts to calculate the magnetic field were abandoned.

However as it was desirable to be able to calculate the strength of the magnetic field at any given point, the measured components of the field were plotted as a function of X,Y and Z, and then mathematical functions were generated which fitted these curves. The form of these functions was limited to some extent by trying to keep them consistent with the known symmetries of the magnetic field. The functions are listed below.

$$B_z = a_0 + a_1 Z^2 + a_2 Z^4 + (a_3 - a_4|Z|)Y^2 - (a_5 - a_6|Z|)X^2 + a_7 \exp.\ (a_8|X| - a_9|Z|)$$

$$B_x = (b_1 - b_2|Z|)X$$

$$B_y = (c_1 + (c_2 - c_3|X|Z^2))Y$$

The expressions are valid with the following range.

$$-13 \leqslant X \leqslant 13$$

$$0 \leqslant Y \leqslant 6$$

$$0 \leqslant Z \leqslant 10$$

where X, Y, Z are measured in cm.

$a_0 = 100$	$a_5 = 0.11$	$b_1 = 10.0$	$c_1 = 10.0$
$a_1 = 0.10$	$a_6 = 0.22$	$b_2 = 0.63$	$c_2 = 0.50$
$a_2 = 0.0051$	$a_7 = 0.25$		$c_3 = 0.02$
$a_3 = 0.52$	$a_8 = 0.75$		
$a_4 = 0.45$	$a_9 = 2.30$		

A brief description of the effect of each term in these expressions follows.

Expression	Term	Explanation
B_z	a_0	This gives the field a normalized value of 100 at the centre.
	$a_1 Z^2$ $a_2 Z^4$	These give the increase in the Z-component with Z.
	$(a_3 - a_4\|Z\|)Y^2$	This term gives the variation with Y (squared because of the symmetry between +Y and -Y). Notice the coefficient of Y depends on $\|Z\|$.
	$(a_5 - a_6\|Z\|)X^2$	Similarly this term describes the variations with X.
	$a_7 \exp.(a_8\|X\| - a_9\|Z\|)$	This term is included to allow for the discontinuity in slope of the sides of the spire at the centre.
B_x	$(b_1 - b_2\|Z\|)X$	The X component of the field is directly proportioned to X, but co-efficient of X depends linearly on $\|Z\|$.
B	$(c_1 + (c_2 - c_3\|X\|)Z^2)Y$	The Y component is directly proportional to Y, but the coefficient depends on both $\|Z\|$ and $\|X\|$.

It must be emphasized that these expressions are not deduced from any physical theory, they are just expressions generated to fit experimental values. A computer (ICT 1301) was used to calculate the field strength as a function of position from these formulae. The values of the constants were adjusted to give a better and better fit. Finally a set of magnetic maps were printed.

Some of the results of these calculations are presented in figs. 4(e), 4(f) and 4(g). The model of the well shown in fig.4(h) was made from the field maps printed out by the computer. Once again a well with a mirror ratio of 1.06 is revealed.

The agreement between the calculated and measured values in the XY planes is poor. This disagreement can be ascribed to the fact that the measurements were made with the probe not positioned exactly in this plane, but at points close to it. Unfortunately the field strength in this region changes very rapidly, so that the measured values give only an approximation to the values in the plane itself.

These expressions for the components of the field will be used to investigate the containment properties of the spire, by running a computer experiment in which the guiding centre approximation is applied.

fig. 4(c) The Magnetic Probe

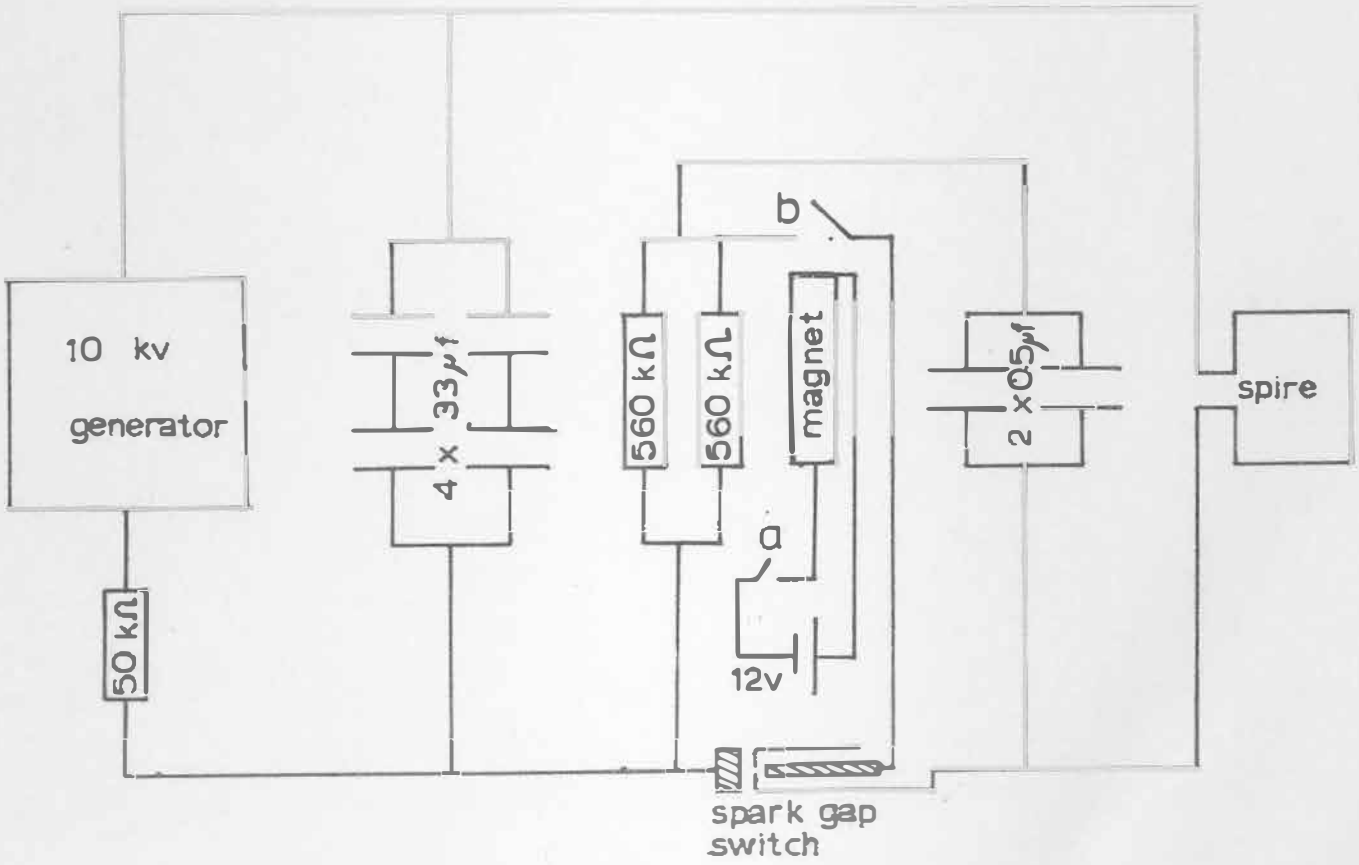

fig 4(a) CIRCUIT DIAGRAM

fig. 4(b) Probe Positioning System

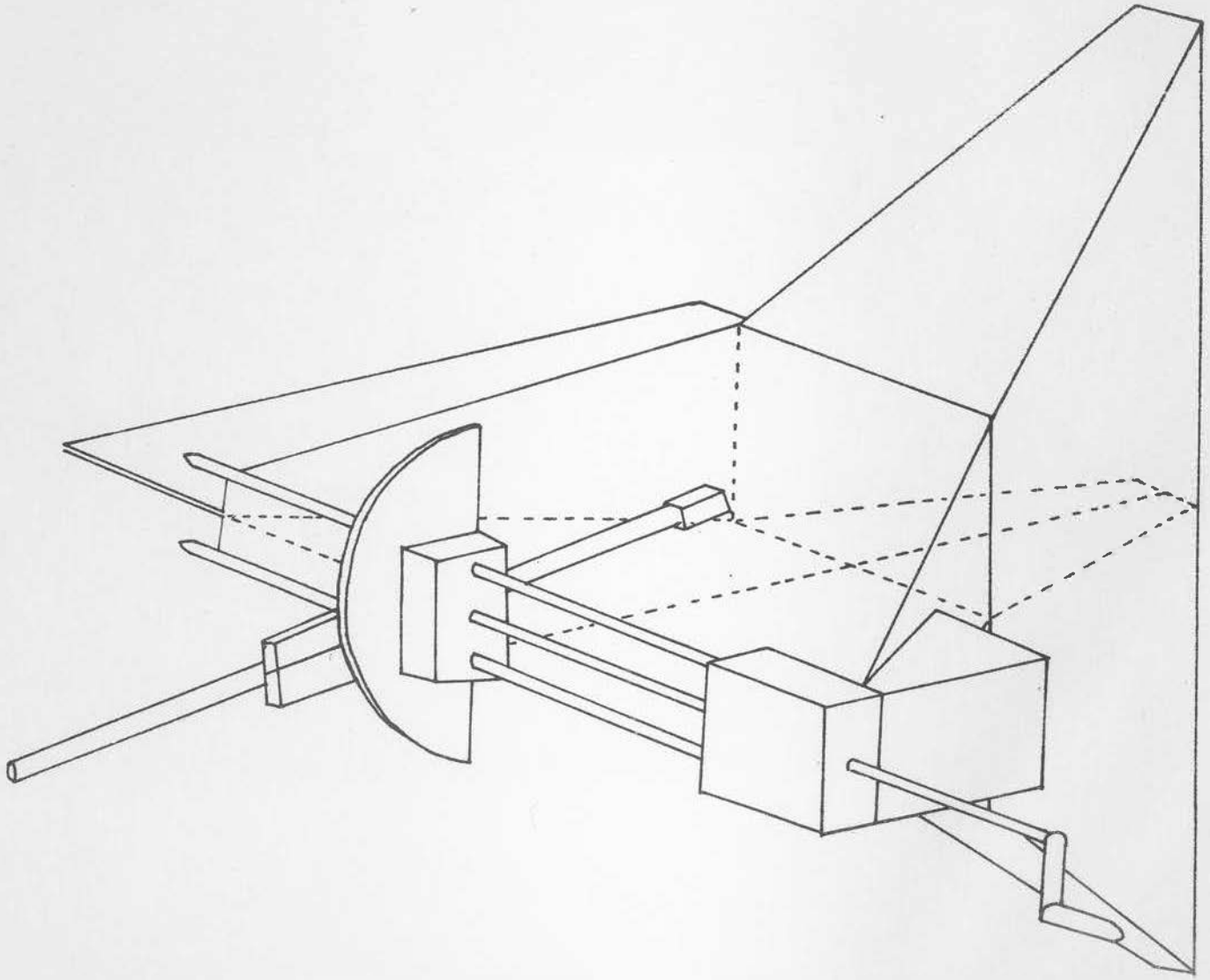

fig. 4(d) Planes in which Measurements were taken

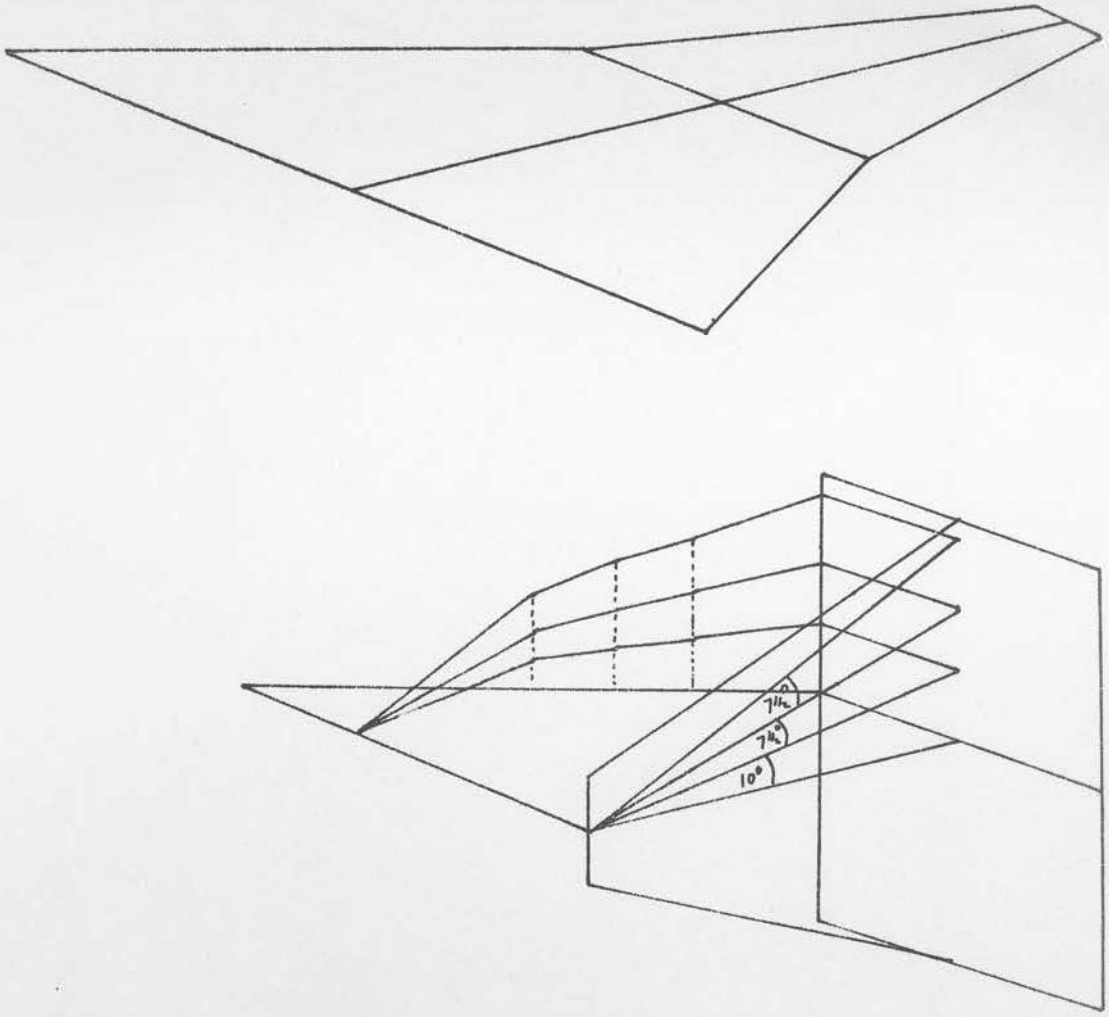

fig. 4(e) Magnetic Field Strength Map in Z = 0 Plane

———— measured

- - - - - calculated

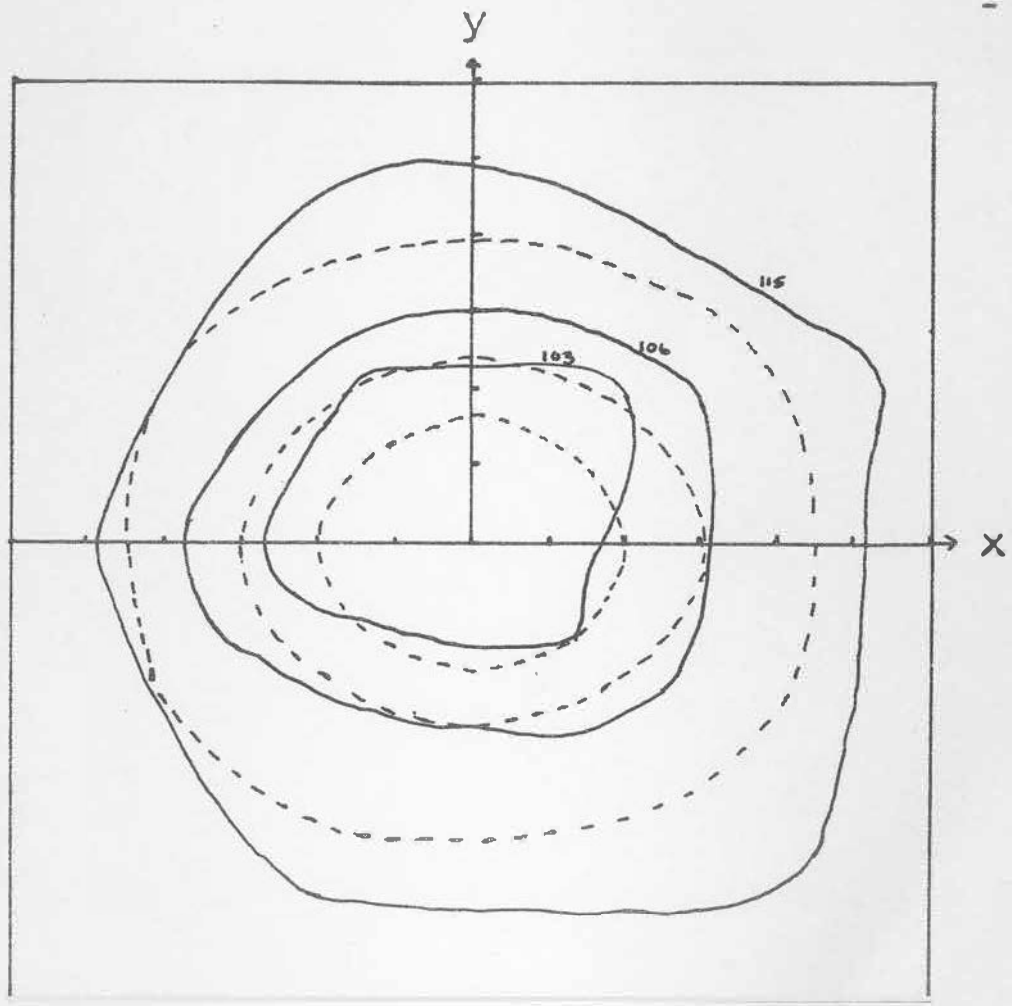

fig. 4(f) Magnetic Field Strength Map in X = 0 plane

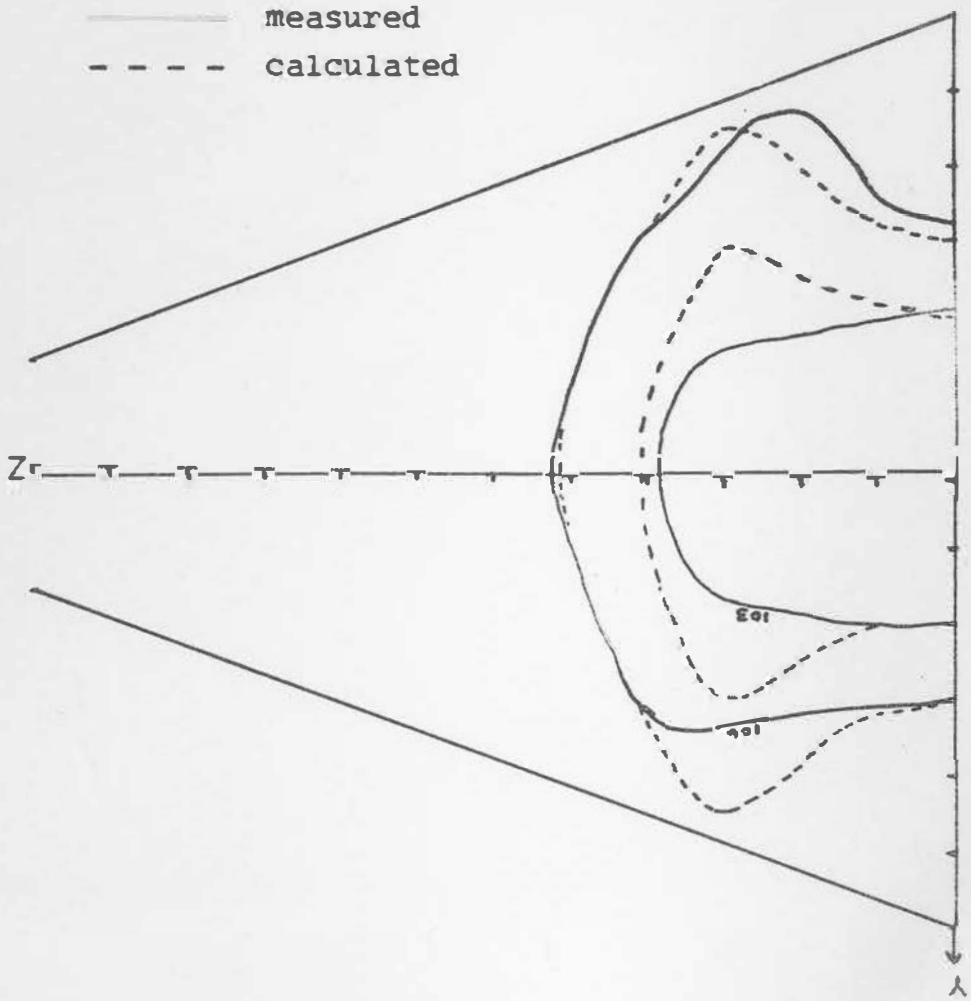

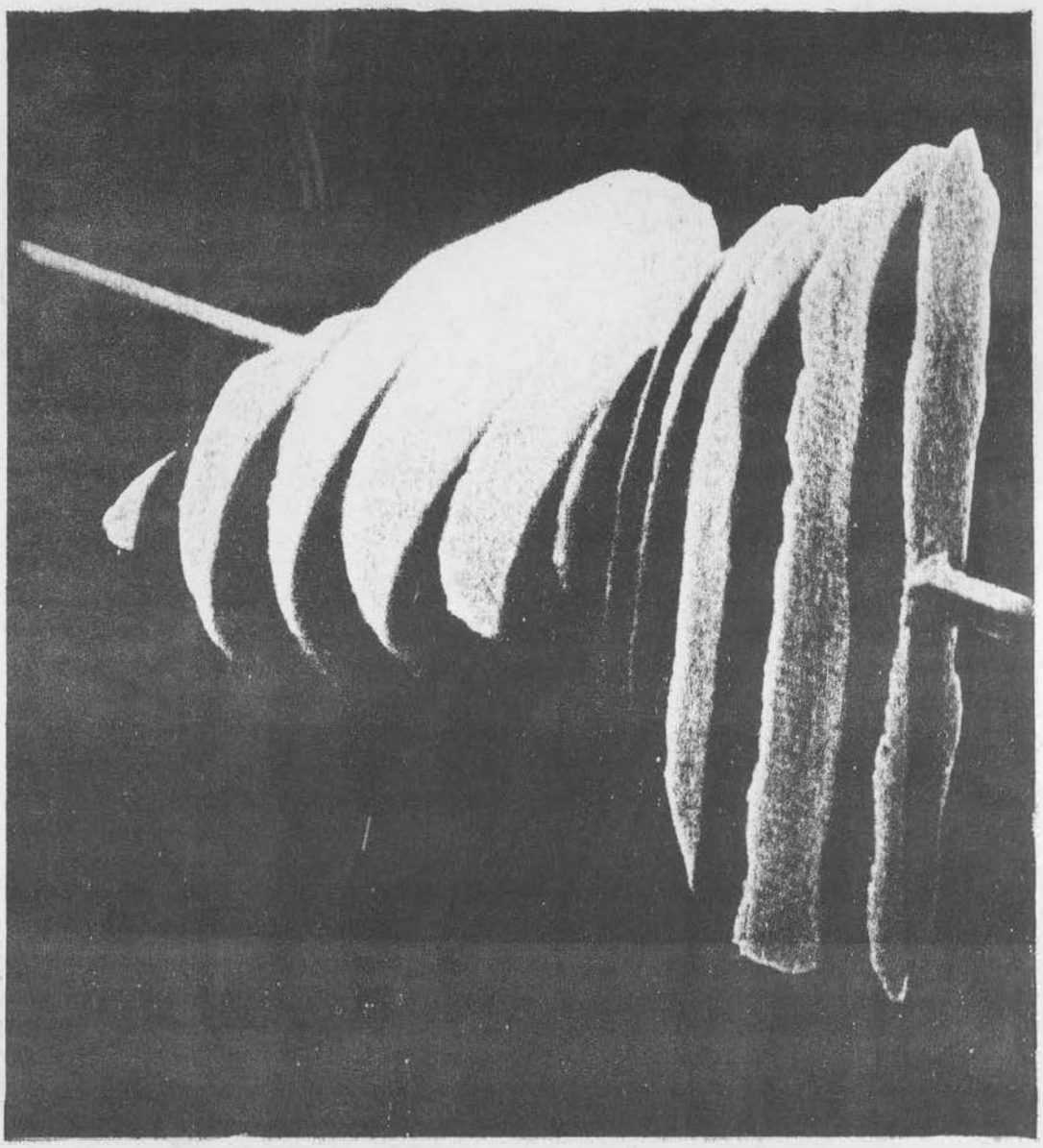

fig. 4(h) A Model of the Well
The envelope of these planes is the limit of the well. Planes are 1 cm apart.

$$J_x = \frac{1}{\mu_0}\left(\frac{\partial B_z}{\partial y} - \frac{\partial B_y}{\partial z}\right)$$

$$J_y = \frac{1}{\mu_0}\left(\frac{\partial B_x}{\partial z} - \frac{\partial B_z}{\partial x}\right)$$

$$J_z = \frac{1}{\mu_0}\left(\frac{\partial B_x}{\partial y} - \frac{\partial B_y}{\partial x}\right)$$

The gas currents should be roughly parallel to the external currents and as our device is a modification of the theta pinch, the external currents will be in the azimuthal direction. We are considering only the Y = 0 plane so we can neglect the J_x and J_z components of the current density and consider only J_y. It turns out that in this device $\frac{\partial B_x}{\partial z} \ll \frac{\partial B_z}{\partial x}$ so we neglect the first term on the right hand side of the expression for J_y and are left with

$$J_y = -1/\mu_0 \frac{\partial B_z}{\partial x}$$

Secondly the magnetic pressure is defined as

$$P_m = \frac{B^2}{2\mu_0}$$

In the central horizontal plane by symmetry considerations, B_y should be zero. This is nearly true in practice except at the beginning of traverses A and B where B_y is

non-zero but still negligible.

So $$B^2 = B_x^2 + B_z^2$$

$$P_m = \frac{B_x^2 + B_z^2}{2\mu_0}$$

Thus simple measurements of the components of the magnetic field will enable both J_y and P_m to be calculated.

5.2 The Magnetic Probe Unit

The probe unit used to measure the magnetic field consisted of three mutually perpendicular coils. Each coil consisted of 25 turns of 46 SWG enamel-covered wire wound on polyethylene bobbins. See fig. 5(a) for dimensions. There was no electrostatic shielding. Each coil was connected to a 47Ω coaxial cable just outside the spire. These connections were made in a steel tube avoid inductive pick-up. The probe was inserted into the vacuum chamber inside a glass tube of external diameter 4.5 mm. A sketch of the entire probe unit can be seen in fig. 5(a).

5.3 Calibration of Coils

In order to get absolute values from these measurements it is necessary to calibrate the coils. The output of a coil in a time varying magnetic field is

$$V_i = n A \frac{dB}{dt}$$

and if a passive integrating circuit of time constant RC, with RC $\gg$ characteristic time of signal is used, the output of the integrator is

$$V_o = (nA)\frac{B}{RC}$$

where nA is the turns area factor. Our calibration process involves finding the effective value of this product.

The coils were calibrated by positioning them in the centre of the magnetic field of a Helmholtz coil and then comparing their integrated outputs with the integrated output of a much larger coil for which the turns-area product can be actually measured. The outputs of the integrators were displayed on a Tektronix 551 double-beam oscilloscope and photographed. After development the amplitude of the peaks of the traces were measured.

The current in the Helmholtz Coil circuit is a damped sine wave. This was the same circuit as used in section 4 except that the spire was replaced by the Helmholtz Coil and the 32μF bank was replaced by a 16.5μF bank.

$$I = I_m e^{-\alpha t} \sin \omega t$$

where $\omega = \sqrt{1/LC - \alpha^2}$

$$\alpha = R/2L$$

$$I_m = V/\sqrt{L/C - R^2/4}$$

The ratio of the current at the first peak to the current at the third peak $\frac{I_1}{I_3} = e^{\alpha \tau}$ when τ is the period. Similarly

$$\frac{I_1}{I_2} = e^{\alpha \tau/2}$$

The amplitudes of the trace peaks will be directly proportional to these currents. If we designate these amplitudes by θ, then:

$$L = \frac{\tau^2}{C\left[4\pi^2 + \left(\ln \frac{\theta_1}{\theta_3}\right)^2\right]}$$

$$\alpha = \frac{\ln\left(\frac{\theta_1}{\theta_3}\right)}{\tau} \quad \text{if } LC \ll 1/\alpha^2$$

Thus from measurements of the period of the discharge and the amplitude of the trace, together with the known

values of the charging voltage V = 2500 volts and capacitance C = 16.5μF, the circuit equation can be solved.

We obtained

$$\tau = 66\ \mu\text{secs}$$
$$L = 6.44\ \mu\text{H}$$
$$I_m = 4.01 \times 10^3\ \text{amps}$$
$$\alpha = 1.86 \times 10^4\ /\text{secs} \quad \text{from } \frac{\theta_1}{\theta_3}$$
$$= 1.62 \times 10^4\ /\text{secs} \quad \text{from } \frac{\theta_1}{\theta_2}$$

For the Helmholtz coils connected in parallel the field at the centre is

$$B = \frac{4\mu_0 n}{5^{3/2} a}\, i$$

where n = 2 and a = 9.4 cm.
Hence at the first current peak we get B = 596 ± 17 gauss (mean from two values of α).

The calibration coil of 10 turns with an effective diameter of 7.78 mm when used in conjunction with a passive integrator (RC = 220μ sec) gave a value of B = 594 ± 20 gauss.

Our final results are given in the following table.

Table 5(i)

Coil	Turns area product (turn - m^2)	
X	4.15×10^{-5}	
Y	3.50×10^{-5}	± 3%
Z	$4.5(5) \times 10^{-5}$	

5.4 The Integrating Circuits

Two pairs of integrating circuits were used with an RC time constant of 47μ sec. Two 5 pole switches were used so that any one or two of the four outputs could be fed into the Tektronix 551 double-beam oscilloscope. These outputs consisted of three integrated signals from the coils and one integrated signal from the current monitor. The current monitor was a coil of approximately 40 turns inserted between the tab plates of the discharge circuit. Diagrams of these integrating circuits are presented in fig. 5(b).

Using the values of table 5(i) and the RC constant one can arrive at the following calibration values for the coils

Table 5(ii)

Coil	B/V_0 $\frac{\text{webers}}{m^2\text{-volt}}$	
X	1.13	
Y	1.35	± 3%
Z	1.03	

5.5 The Discharge Circuit

The layout of the circuit is essentially the same as in fig. 3(a), except for the following minor differences. The 33μF bank is replaced by 39 one microfarad capacitors connected in parallel, the triggering bank is replaced by a single 1μF capacitor, and the resistors have different values appropriate to the new conditions. In the table below the operating parameters of the system are given.

Table 5(iii)

Capacitance (μF)	39
Charge voltage (KV)	7
Stored Energy (J)	955

contd.

Table 5(iii) - continued.

Total Inductance (nH)	65
Discharge period (μsec)	vacuum 10.2
Peak Magnetic Field (gauss)	~4000
Coil Inductance (nH)	39.5
Initial Gas Pressure (μ)	20
Gas Used	Atmospheric air

5.6 The Experimental Procedure

The measurements were confined to the central horizontal plane (Y = 0). The glass tube in each case was positioned so that it extended right across the vacuum chamber, touching the far wall. The probe was positioned at the appropriate points on the chosen traverse inside the tube. (See fig. 5(c)). The chamber was then pumped down and the leak rate adjusted so that a dynamic pressure equilibrium was maintained at 20μ. The gas was lightly preionized with a small tesla coil. With the tesla coil operating the main bank was discharged. The outputs of the coils and monitor were displayed on the

double-beam oscilloscope in the following pairs: (1) Z coil and current monitor, (2) X coil and Y coil. The traces were photographed. After discharge the chamber was pumped down and then refilled to 20μ pressure, where the shot was repeated or the probe moved to a new position.

After development the photographed traces were projected onto a sheet of graph paper and traced at their original size. The amplitude of the trace at every $\frac{1}{2}$ microseconds in the interval $5 \rightarrow 15$ microseconds was measured and recorded.

These values were punched onto cards. Two programs were written to calculate J_y and P_m respectively. The print out was arranged so that the calculated values were printed at their coordinate points. Thus contour maps could be drawn directly on the computer print-out sheets. The University's ICT 1301 computer was used to perform the calculations.

5.7 Errors

The most serious error that could appear in this experimental procedure is irreproducibility of the measure-

ments. Fortunately the magnetic measurements were very reproducible. It is unusual for traces to differ enough, so that, when they are superposed, as difference between them is detectable. The slight shot to shot variations compounded with the small reading errors should be easily covered by our criterion that all results originating from amplitude differences of less that 1 mm on the traces would be ignored. In our case this criterion leads to variations of the order of 5 - 10%. Hence this source of error is much greater than any calibration error.

fig. 5(a) The Magnetic Probe

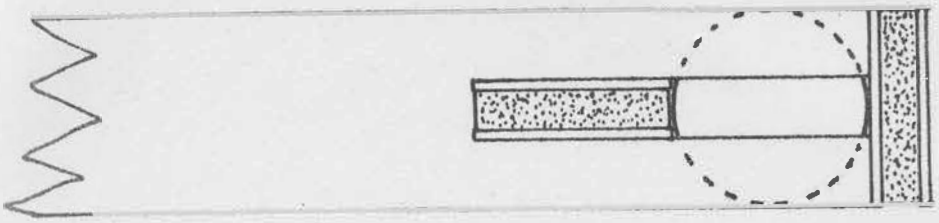

1mm

fig. 5(b) The Integrating Circuits

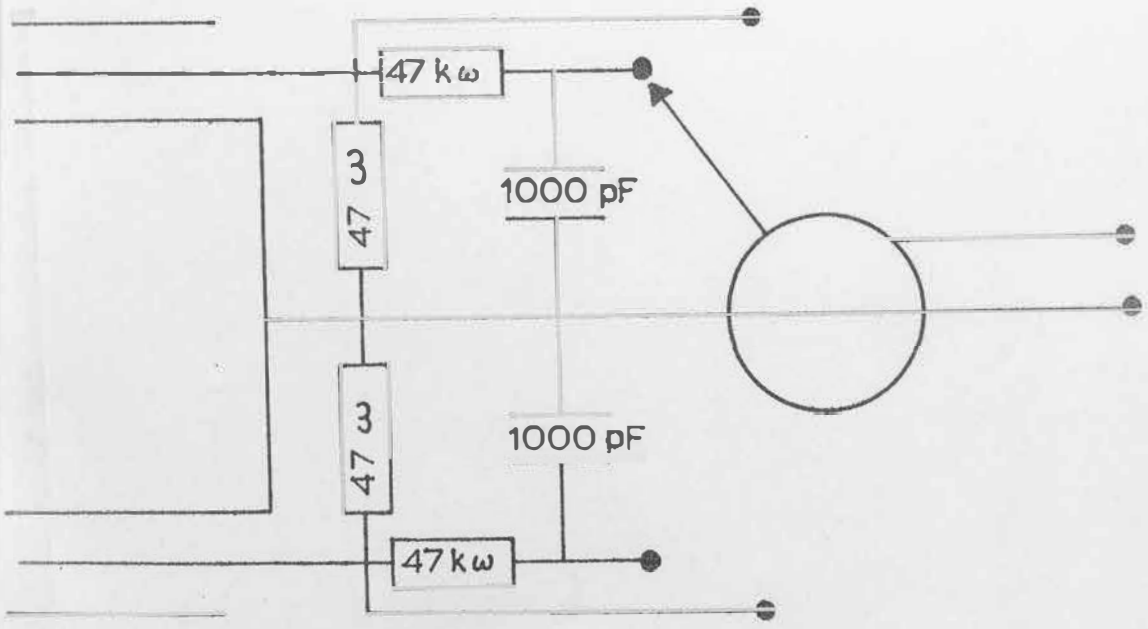

fig. 5(c) Probe in Vacuum Chamber

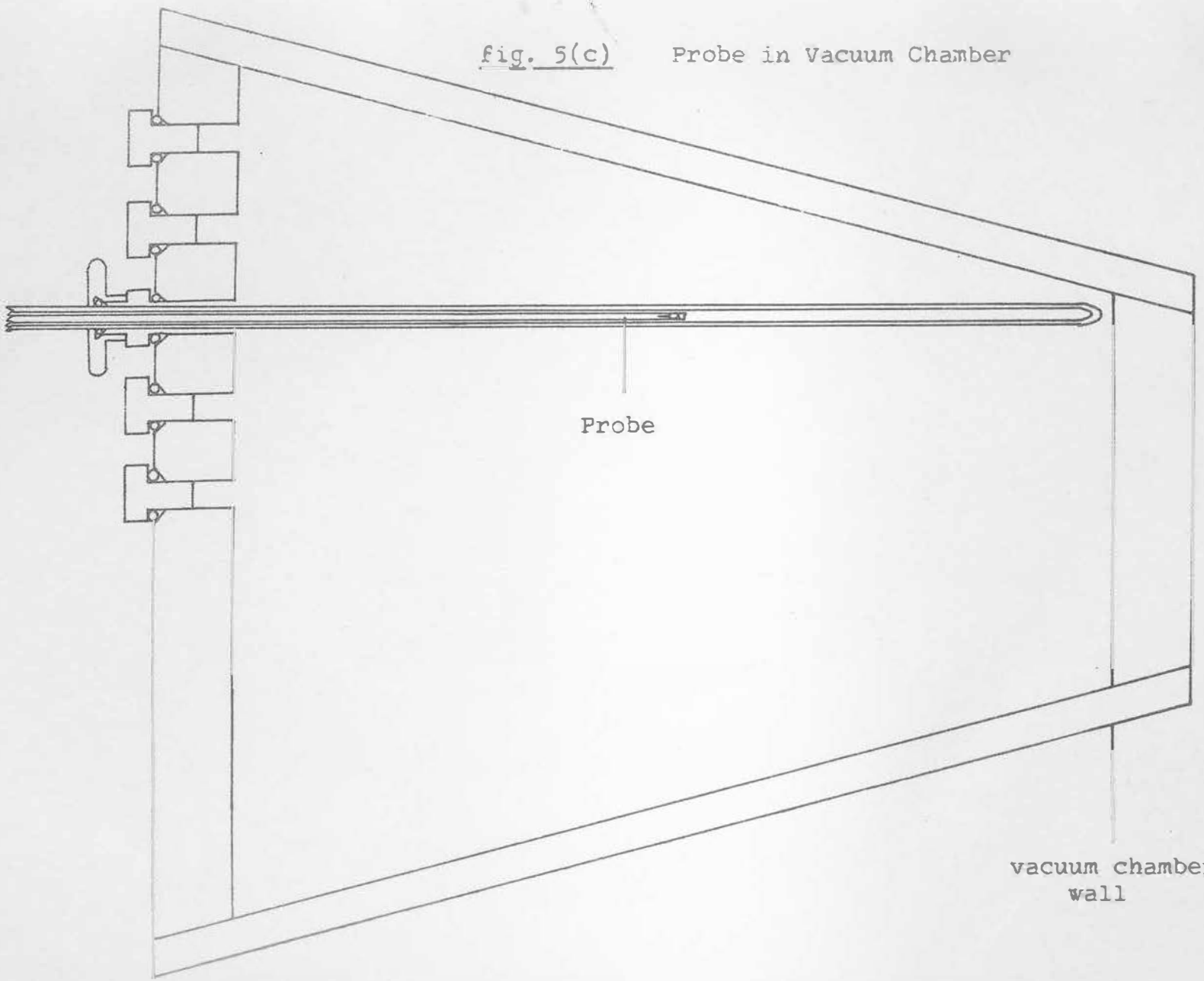

fig 5(d) Positions at which Measurements were taken

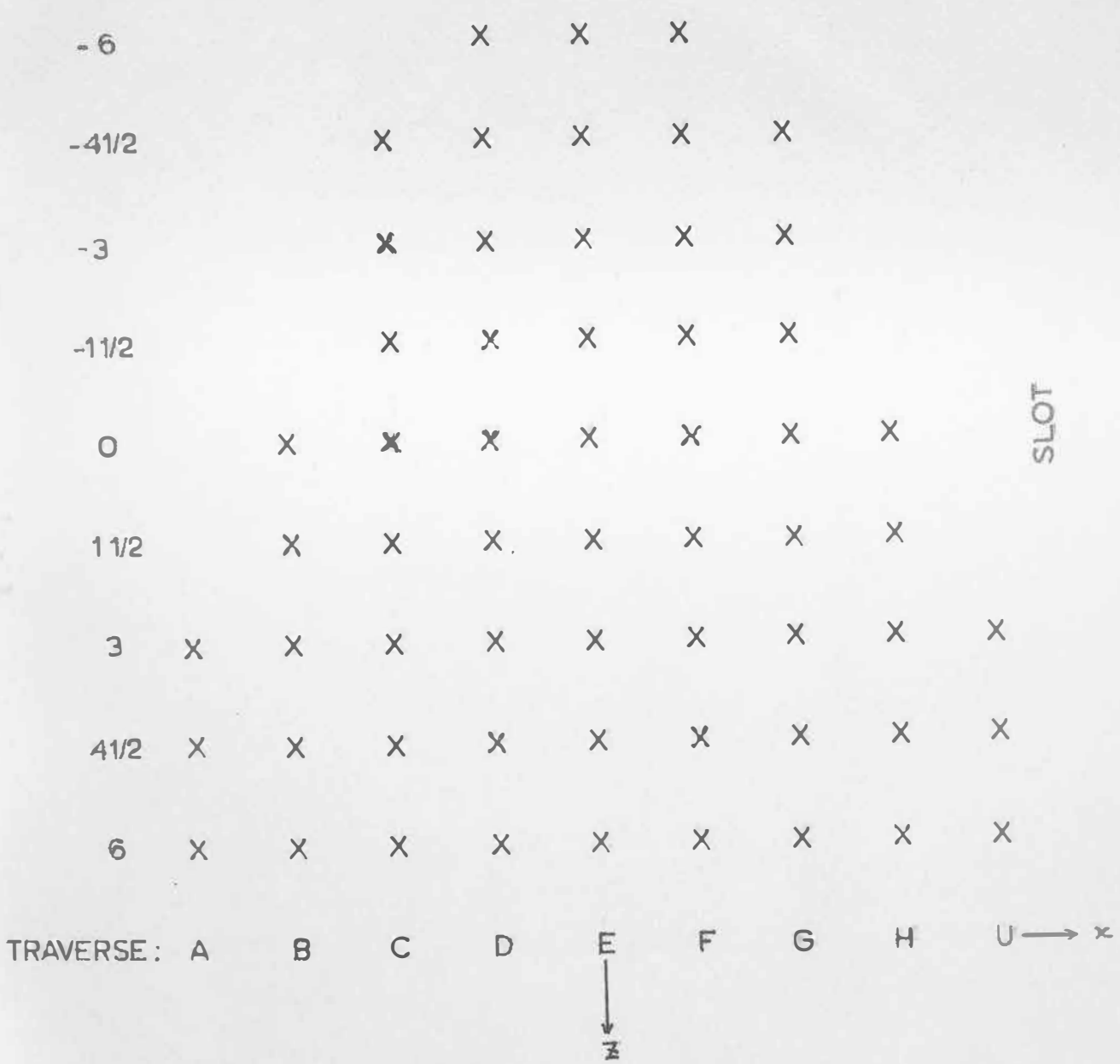

SECTION 6

THE ELECTRON DENSITY

6. ELECTRON DENSITY MEASUREMENTS

6.1 If in a plasma the electrons carry a current in a magnetic field they will be subjected to a Lorentz force of $\underset{\sim}{J} \times \underset{\sim}{B}$. This force tends to move them away from ions. The separation of charges induces a large electric field, E. The field accelerates the ions and the Lorentz force is transmitted to the ions through this electric field. Now with a very good approximation we can equate the Lorentz force density to the Coulomb force density for the ions.

$$\underset{\sim}{J} \times \underset{\sim}{B} = Z n_i e \underset{\sim}{E}$$

where Ze is the average ionic charge and n_i is the ion density. This is the same for a neutral plasma as

$$n_e e \underset{\sim}{E} = \underset{\sim}{J} \times \underset{\sim}{B}$$

$$= \begin{vmatrix} i & j & k \\ J_x & J_y & J_z \\ B_x & B_y & B_z \end{vmatrix}$$

and we end up with three equations for the electron density.

$$n_e = \frac{1}{e E_x} \left[J_y B_z - J_z B_y \right]$$

$$n_e = \frac{1}{e E_y} \left[J_z B_x - J_x B_z \right]$$

$$n_e = \frac{1}{e E_z} \left[J_x B_y - J_y B_x \right]$$

In our central horizontal plane B_y is nearly always zero. Secondly if the only significant component of the current density is J_y, then we have the two reduced equations.

$$n_e = \frac{J_y B_z}{e E_x} \qquad (1)$$

$$n_e = -\frac{J_y B_x}{e E_z} \qquad (2)$$

5.2 If we can measure the electric field then we shall be able to calculate the electron density because we know J_y, B_x and B_z. The method used by Lovberg (1) to measure the electric field was a floating double electric probe. We must see if a floating probe will assume the plasma potential of its immediate neighbourhood.

Consider a plasma with a maxwellian velocity distribution for the electrons and stationary ions. Stationary here means the ions have zero velocity where the potential due to the probe is zero. Then the electron current density to the probe is

$$j_e = j_r \exp(-e\phi_s/kT_e) \qquad (3)$$

where j_r = the random electron current density

ϕ_s = sheath potential

k = Boltzmann's constant

e = electronic charge

T_e = the electron temperature

As we have a maxwellian velocity distribution $n\left(\frac{kT}{2\pi m}\right)^{1/2}$ particles will strike unit area per second. Therefore the random electron current density is

$$j_r = e n_e \left(\frac{k T_e}{2\pi m_e}\right)^{1/2} \qquad (4)$$

We can use an expression derived by Allen et al (2) for the ion current density to a plane probe.

$$j_i = 2^{-1/2} \exp(-1/2)\, n_i e \left(\frac{kT_e}{m_i}\right)^{1/2} \qquad (5)$$

Then the net current density can be obtained by combining (3), (4) and (5)

$$j = 2^{-1/2} \exp(-1/2)\, n_i e \left(\frac{kT_e}{m_i}\right)^{1/2} - e n_e \left(\frac{kT_e}{2\pi m_e}\right)^{1/2} \exp\left(\frac{-e\phi_s}{kT_e}\right)$$

This can be reduced to

$$j = e n \left(\frac{kT_e}{m_i}\right)^{1/2} \left[2^{-1/2} \exp(-1/2) - \left(\frac{m_i}{2\pi m_e}\right)^{1/2} \exp\left(\frac{-e\phi_s}{kT_e}\right)\right]$$

$n_i = n_e = n$

We wish to see what the sheath potential will be for a given current density drawn by our probe.

Re-arranging

$$\phi_s = -\frac{kT_e}{e} \ln\left[\left(\frac{m_i}{2\pi m_e}\right)^{1/2} 2^{-1/2} \exp(-1/2) - \left(\frac{kT}{2\pi m_e}\right)^{-1/2} \frac{j}{ne}\right]$$

and

$$\phi_s = \frac{kT_e}{e}\left[\ln\left(\frac{m_i}{2\pi m_e}\right) + 1\right]$$

if

$$2^{-1/2}\left(\frac{m_i}{2\pi m_e}\right)^{-1/2} \exp.(-1/2) \gg \left(\frac{kT_e}{2\pi m_e}\right)^{-1/2} \frac{j}{ne}$$

Neglecting the factor

$$2^{-1/2} \exp.(-1/2)$$

we get

$$ne\left(\frac{kT_e}{m_i}\right)^{1/2} \gg j$$

For our plasma the left hand side is of the order of 10^5 and as we shall draw current densities of the order of 1 amp/meter^2 the condition is easily satisfied. Hence we can use the reduced expression for the sheath potential.

This sheath voltage will occur at both electrodes of the probe and hence the potential difference measured by the probe (V_M) will differ substantially from the difference

between the plasma potentials in the neighbourhood of each electrode only if the electron temperature differs appreciably for each electrode. We want

$$V_n \gg \frac{k}{e}\left[T_{e_1} - T_{e_2}\right]$$

$$\frac{V_n e}{k} \gg \Delta T$$

With measured voltages of the order of 10^2, we have

$$10^6\ ^\circ K \gg \Delta T$$

This condition would also easily be satisfied in our plasma.

We can conclude by saying that if we insert a floating double probe into the plasma, providing the current density drawn is small, each electrode will assume the plasma potential of its neighbourhood minus a factor the order of $\frac{kT_e}{e}$.

Now we can return to our original equations. As equation (2) can be applied with a simpler experimental system we chose to work with it.

In Section 4 we have obtained the necessary values of B_x and J_y and so all that remains is to measure E_z. The general layout of the experimental system can be seen in Section 3.

6.2 The Probe and Pulse Circuit

A floating electrical probe was constructed. The construction details and dimensions can be seen in fig. 5(a). The signal from the probe was fed into an RC voltage divider in which the values of C were adjusted to give minimum distortion at the ringing frequency of the external discharge circuit. From the output of the voltage divider the signal passed through a 47ω coaxial cable to a ferrite core pulse transformer (see fig. 5(b)). The turns ratio of the the transformer was 1 : 1 with a self inductance L for both primary and secondary of 1.6 mH. The resistance R of both windings was of the order of one ohm while the primary to secondary capacitance was 72pF. This pulse transformer was included to isolate the plasma from earth.

Calibration of the Probe Circuit

As the probe itself produced no appreciable distortion or attenuation, it was removed from the circuit and only the voltage divider, pulse transformer and intermediate cables were calibrated.

Fig 6(b) Voltage Divider and Pulse Transformer.

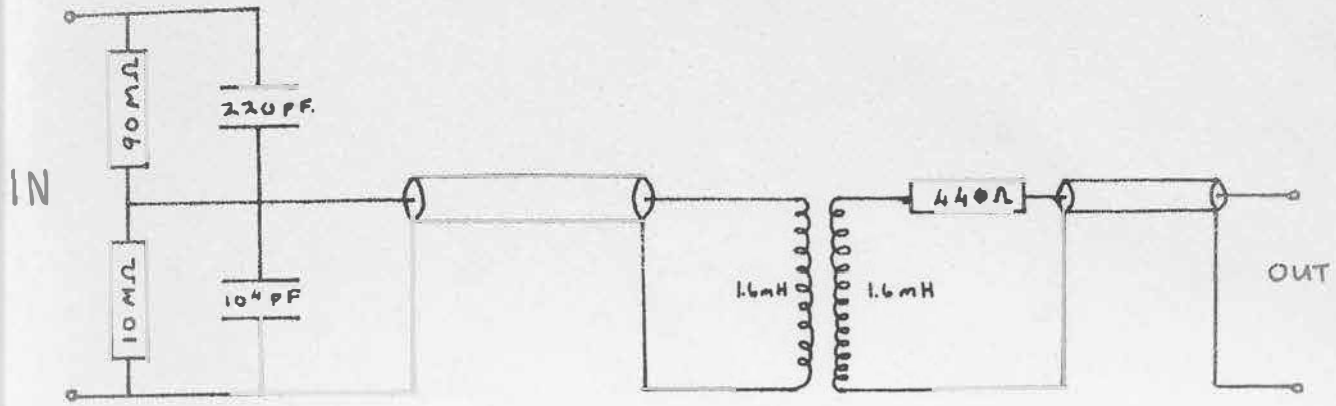

The input of the voltage divider was connected to an oscillator and the output of the cable leading from the pulse transformer was fed into a double-beam oscilloscope. The second beam of the oscilloscope carried the output signal of the oscillator. From the amplitude of these two traces it was possible to get an attenuation coefficient $\alpha = \frac{V_{OUT}}{V_{IN}}$. The frequency of the oscillator was set at a number of fixed frequencies in the range from 4kHz to 512kHz and a plot of attenuation coefficient against the log of the oscillator period was produced (see fig. 5(d)). The attenuation coefficient was roughly constant, $\pm$ 8%, for frequencies ranging from 25 kHz to 400 kHz. The approximate value of the attenuation coefficient, 2×10^{-3}, in this

range was used in all subsequent calculations as the floating probe output was very near to the ringing frequency of the discharge circuit i.e. 100 kc/s. Any high frequency peaks that did occur however would be highly attenuated.

6.3 Measurement Procedure

We wished to measure the z-component of the electric field E . If the potential difference between the probes is measured and we know the distance between the probes we can find the electric field E_z

from $$E_z = - \frac{V_{1,2}}{d}$$

Where $V_{1,2}$ is the potential difference between the probes and d is the distance between them.

The double probe was inserted into the vacuum chamber as was the magnetic probe in fig. 4(c). After pumping down, air was allowed to leak in until a dynamic pressure equilibrium was obtained at 20μ. The preionizer was started and then the main condenser bank was discharged. This bank was identical to that used in Section 4. One trace on the Tektronix 551 double-beam oscilloscope recorded the potential difference between the two probes, while the second displayed

the output of the current monitor. These two traces were photographed. After each discharge the chamber was flushed out three times by allowing the air pressure to increase to several hundred microns and then pumping down to a base pressure of about one micron. We found this to be necessary because the electric probe signals seemed to be very sensitive to impurities. As the vacuum chamber was made of perspex, it became very polluted after each discharge. Three discharges were made with the probe in single position, before moving on to the next measuring point.

After development the traces were projected onto graph paper and traced at their original size. Then the amplitude of the trace was measured and recorded in steps of a half microsecond from 5μsec to 15μsec after the firing of the main bank.

6.4 The Calculation of the Electron Density

A program was written to calculate the values of the electron density and print out these values at their co-ordinate points. Firstly J_γ was calculated. Then the

average value of the B_x and the average of the E_z components were evaluated (See fig. 6(c)). The E_z components presented some difficulty. If the trace amplitude had been impossible to read, it was assigned the value zero. Hence when calculating the average E_z, the computer was instructed to ignore values of zero when calculating the average.

A value for n_e was not calculated if any of the components J_y, B_x, E_z fell within their noise level. When this occurred the computer printed out 'xxxx' instead of a value for n_e. Because of the symmetry of the device the B_x components were too small on the central traverses to get above the noise criteria and it was only in the actual gas current sheath that the values of J_y were sufficiently large. Thus it was that the calculation only produced values for n_e in the gas current sheath at points away from the z-axis, although this might not be the only region where high electron densities occur.

Below is the unit cell in which measurements were made and where the calculated values have meaning. The barred

values are those values used with J_y in the calculation of n_e.

fig 6(c) Unit Cell for Calculations

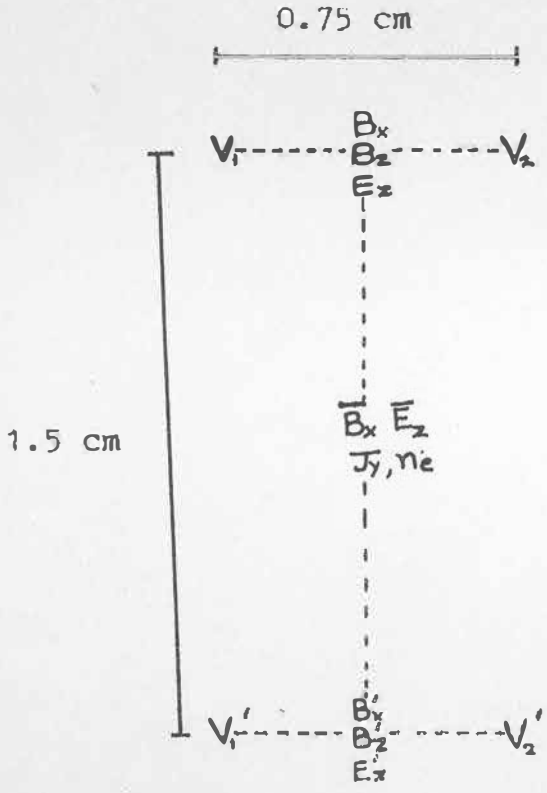

$$\bar{B}_x = \frac{B_x + B'_x}{2}$$

$$\bar{E}_z = \frac{E_z + E'_z}{2}$$

iff $E_z \neq 0$

$E'_z \neq 0$

$$J_y = -\frac{1}{\mu_0}\left[\frac{B_z - B'_x}{\Delta x}\right]$$

$\bar{E}_z = E_z$ if $E'_z = 0$

$\bar{E}_z = E'_z$ if $E_z = 0$

fig. 6(a) The Double Floating Probe

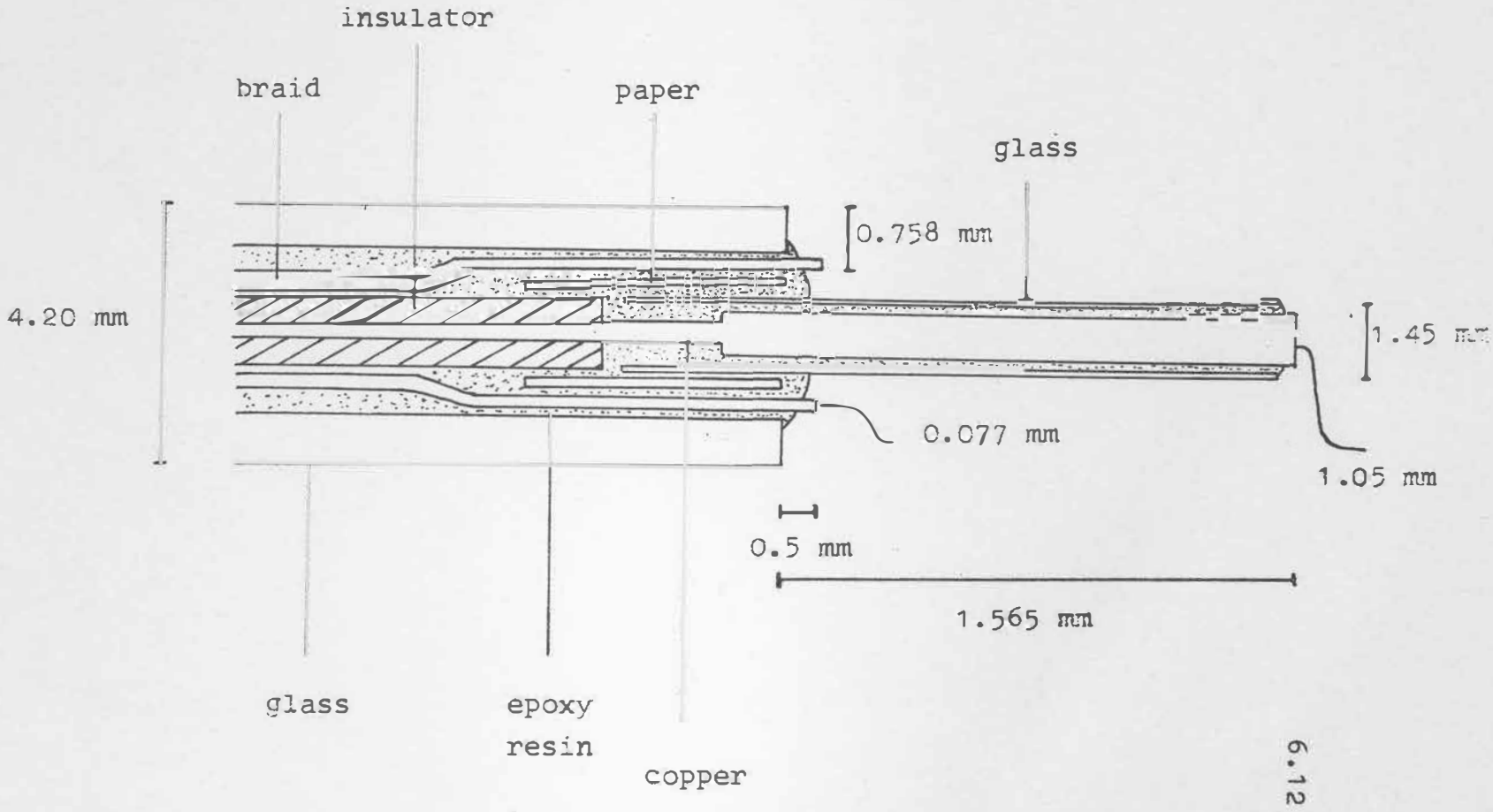

6.12

fig 6(d).

Plot of attenuation coefficient as a function of period of signal

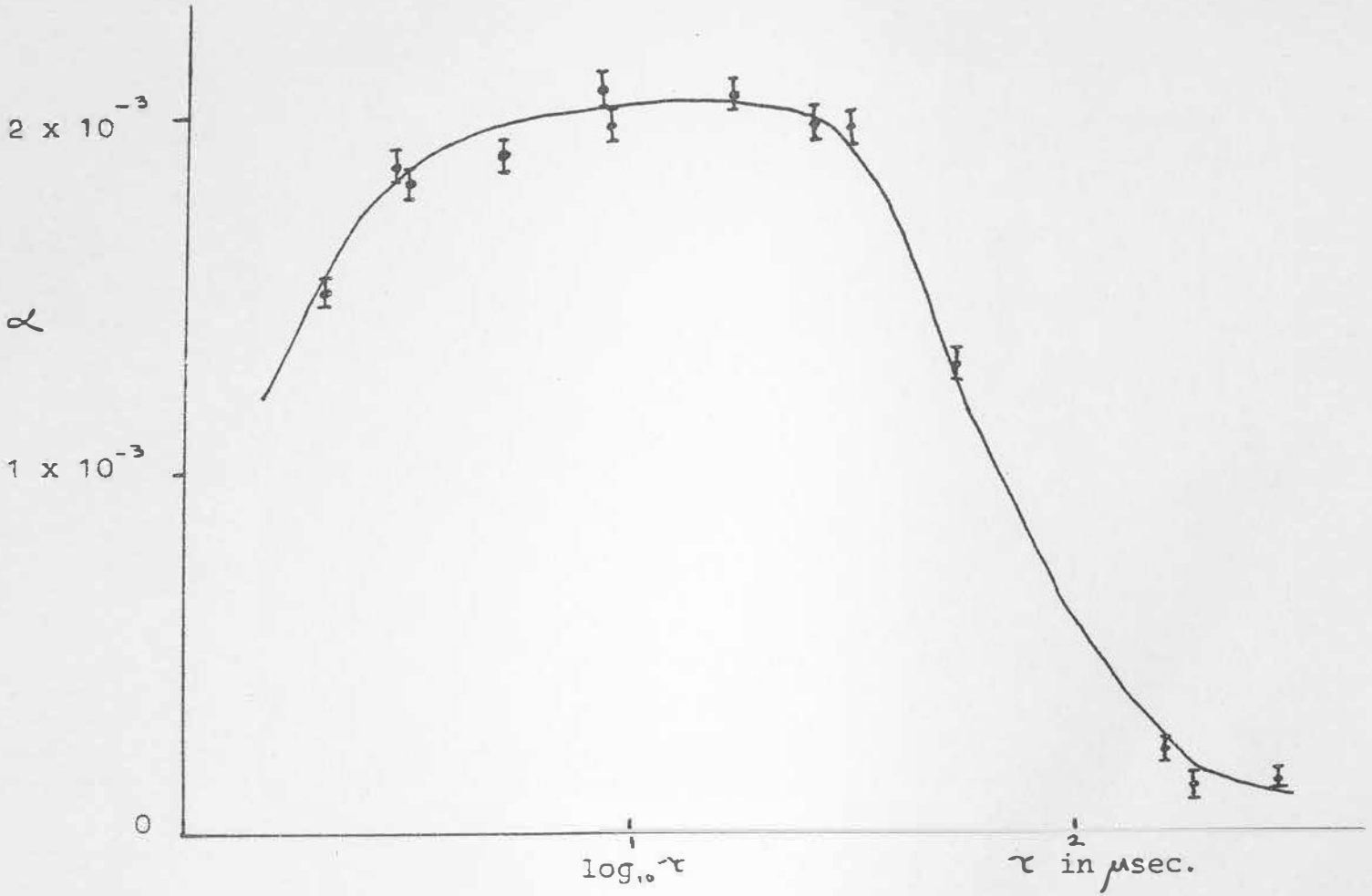

SECTION 7

DISCUSSION

7. DISCUSSION OF EXPERIMENTAL RESULTS

7.1 In this section an attempt will be made to analyse the experimental results and to use them to put together a coherent description of the plasma dynamics within the spire in the Y = 0 plane.

As our measurements were made at every $\frac{1}{2}$ microsecond in the interval 5 to 15 microseconds after the firing of the main condenser bank, we shall measure time in half microseconds and begin the description at t = 10 half-microseconds.

7.2 The Second Half Cycle

At t = 10, just before the end of the first half cycle of the external current, the first signs of gas breakdown became apparent (Traces 1,2). Soon after the external current has reversed a gas current sheath appears near the slot of the device with a return current sheath on the axis. Between these sheaths a small amount of reverse flux is trapped. Later at least three gas current loops appear to be present in the Y = 0 plane. The diamagnetic effect of

the plasma exludes the increasing magnetic field from the central region (see Graph 2). The gas currents reach their peak at t = 13 → 14. At t = 14 the diamagnetic effect begins to break down and the external strong field penetrates rapidly to the central region. It can be seen that the magnetic pressure outside the sheath reaches its peak before the external current reaches a maximum. This probably occurs because the rising field is trapped between the spire wall and the gas current sheath and so compressed. Later when the sheath moves inwards the compression is relaxed and the pressure decreased (see Graph 2). The electron density during this compression phase reaches maximum at t = 13, of 1.3×10^{14} electrons/cc. Suddenly at t = 15 the chaotic three current loops have disappeared and two well developed parallel current sheaths appear along the line X = 2 and X = -2. The current has reversed direction and the sheath on the side opposite the slot carries the highest current density. The magnetic field inside the sheath is now higher than outside it. When the high external magnetic field penetrates to the interior it is further compressed (see Graph 2) reaching a maximum value with the external

current at t = 16. For the next microsecond the sheath maintains its position although the current density drops from 5×10^{6} to 2×10^{6} amps/m^2 and two small high magnetic pressure regions are maintained on the Z axis at Z = 2 and Z = $-1\frac{1}{2}$. The electron density is about 3×10^{14} electrons/cc. At t = 18 the sheath moves out to the walls, but still maintains a high interior field while the external field decreases. This effect can be seen in the traces 1 and 2 where the B_z trace does not go to zero as quickly as does the current monitor trace. At the close of the half cycle, t = 20, the current densities begin to increase again as the external current nears reversal.

7.3 The Third Half Cycle

An almost complete picture of the dynamics of this half cycle is presented in the diagrams of this section. When the external current is zero at t = 21 the gas current densities increase very rapidly at the walls of the vacuum chamber. Owing to these high currents the entire central region is filled with trapped reverse flux. Slowly the

gas current sheath moves inwards while a large magnetic pressure builds up behind it. Once again the external pressure reaches a peak before the external current because the rising flux is compressed between the spire walls and the conducting plasma sheath. The current densities rise to 17 x 10^6 amps/m^2 and the electron density is 2 x 10^{14} electrons/cc at t ≈ 25. Meanwhile the trapped reverse flux has been decreasing steadily and finally disappears on the axis at t = 26 (see Graph 2). At approximately t ≈ 26 the current sheath moves in very rapidly and all the trapped reversed flux has disappeared. The high external magnetic field penetrates rapidly (see traces 1,2). In fig. 7(a) a set of isochronous curves show the rates of penetration of the external field. Just after t = 27 the sheath currents drop to zero, but the sheath obviously keeps moving in because when the gas currents reappear at t = 28 with current reversed, the sheath is nearer the centre. Now the high pressure field is trapped inside the sheath while the external field decreases. In fact the trapped field is even compressed to some degree (see Graph 2). At t = 29 the sheath swings towards the walls where the co-ordinates have negative Z values. Another sheath with

currents flowing in the same direction appears at the slot, while for positive values of Z the inner sheath persists. Finally at t = 30 a large diffuse current sheath grows at the walls and remains there for the duration of the discharge.

7.4 Remarks on the Graphs and Diagrams

1. No current density values are plotted before t = 15 because three current loops exist before this time and it is not possible to refer unambiguously to the sheath near the slot and to the sheath on the far side.

2. At time t = 15 the gas current and the external current are in the same sense.

3. The average values for the external and internal magnetic pressures in Graph 2 are not strictly calculated means but rather rough average values.

4. In all the diagrams the slot of the device is on the

bottom edge of the diagram. The thick black edge represents the inner wall of the vacuum chamber.

5. Below is the code to the contour shading.

Shading	J_y amps/m^2 x 10^6	P_m newton/m^2 x 10^3	N_e electron/cc x 10^{14}
	+3.6 → +10.5	12 → 24	1 → 5
	-3.6 → -10.5		
	above +10.5 below -10.5	25 → 36	6 → 10
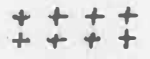	+2.0 → +3.5		above 10
	-2.0 → -3.5		

7.5 Conclusion

In a summary it may be said that we have investigated a modified theta-pinch proposed by J. Andreoletti and shown that it in fact does give rise to a magnetic well. We have completed a preliminary survey of the plasma dynamics in the central horizontal plane of the device with magnetic and floating electric probes. These investigations have produced a fairly clear picture of the plasma motion in

the central horizontal plane. Our time resolution is not good enough to explore fast transitions such as the penetration of the high external field when the gas current drops to zero. However the time resolution tends to be limited rather by the experimenter's industry than the diagnostic techniques that were used, as he had to act as a human analogue to digital converter.

Most encouraging results were obtained from the floating electrical probe method developed by Lovberg. The electron densities obtained tend to be consistent with the other information we have about the plasma.

One most important point must be mentioned. At no time do we actually test the minimum-B properties of the device. We did not have a plasma injection system so we could not operate in the $\beta = 1$ mode. The adiabatic mode was not open to us either as we had to rely on the electric field of the external circuit at current zeroes to ionize the gas. The current sheath formed at the walls then gravely distorted the magnetic field. During the

compression phase of each half cycle the diamagnetism of the plasma keeps the internal field strength low. Once the high field has penetrated, the diamagnetic effect preserves the high field in the interior, creating the reverse of a minimum-B situation.

Many improvements of the experimental system come to mind. It would certainly help to have a cleaner plasma by using a glass walled vacuum chamber. Also an injected plasma or one produced by a preionizing Z pinch would remove the initial chaotic post break-down condition and enable the strong magnetic field of the first half cycle to be used profitably. Then it would be possible to test the minimum-B properties of the device. To do this, the main discharge circuit needs to be crowbarred at the peak of the first half cycle so that changes in the external field are slower and some serious investigation of the containment properties of the device can be made. Lastly, if the floating probe measurements were made through

ports in the wall of the spire itself so that equation (1) of Section (5) could be used, better results could be expected as B_z is inherently easier to measure than B_x.

fig 7(a)

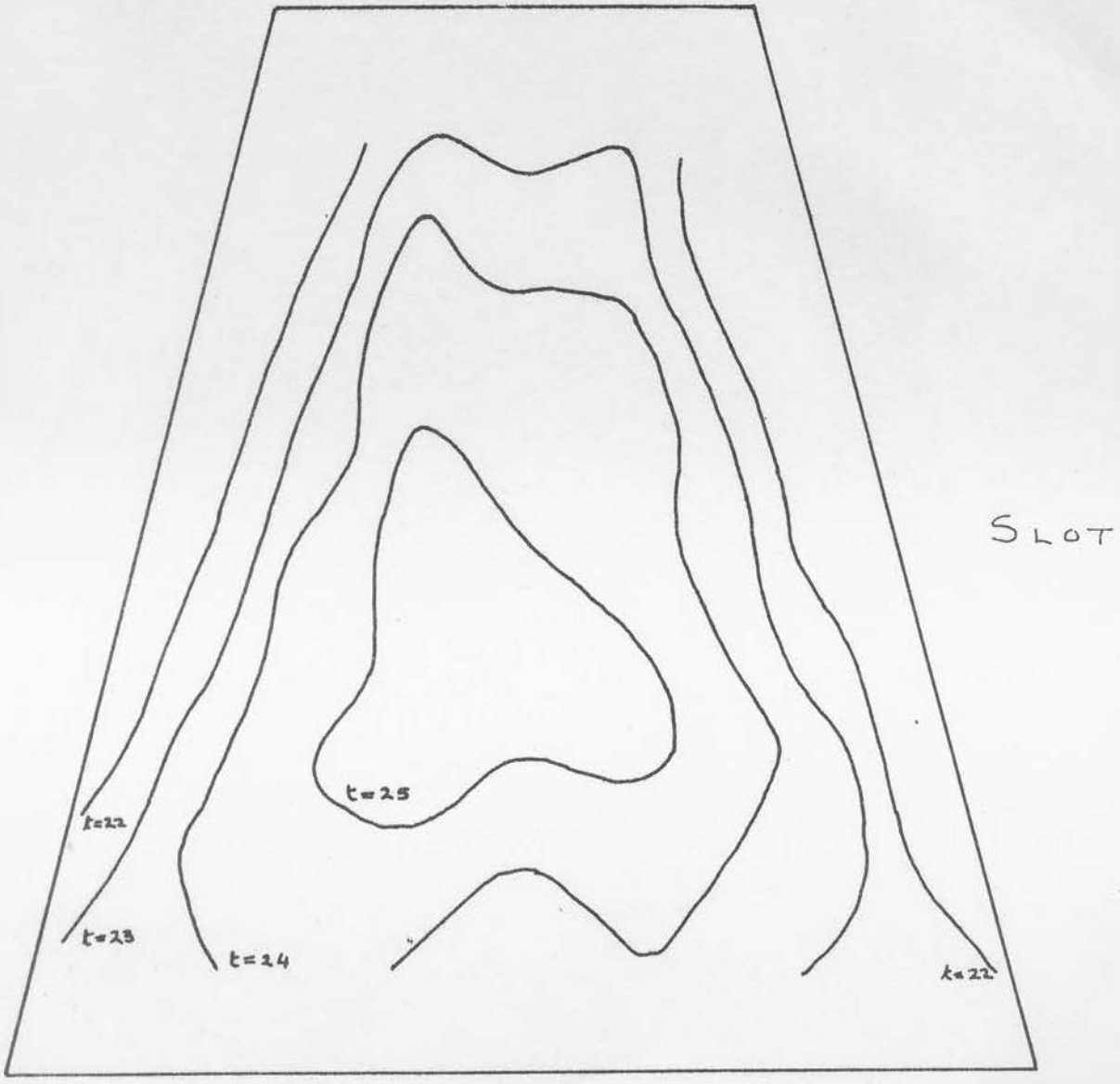

A set of isochronous curves showing when and where in the Y = 0 plane the trapped reversed flux in the third half cycle disappears.

GRAPH 1

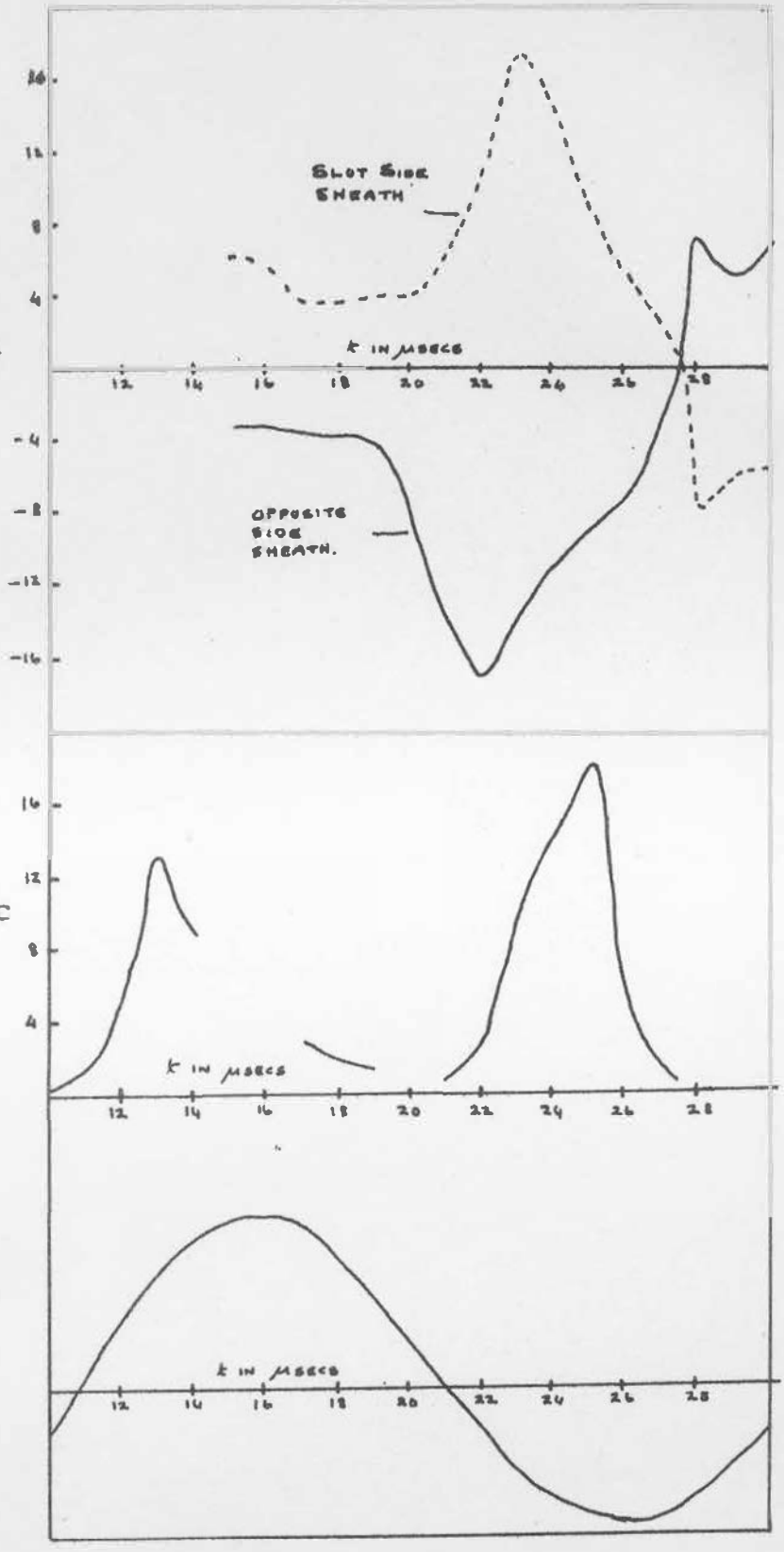

J_y max in amps/m^2 x 10^6

N_e max in elec./cc x 10^{14}

I_{ex} in arb. units

TIME

GRAPH 2

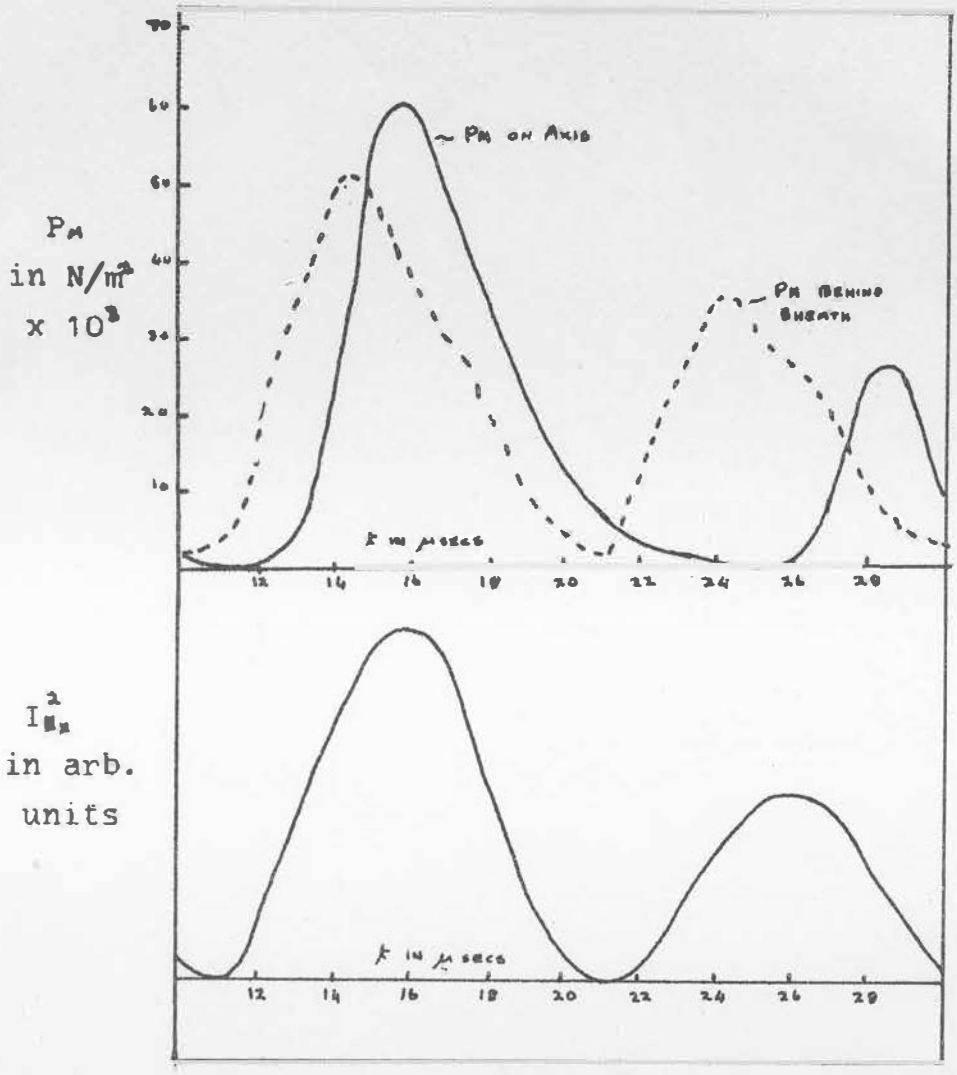
P_M in N/m^2 x 10^3
~ P_M on Axis
P_M Behind Breath
t in μsecs
12
14
16
18
20
22
24
26
28
$I^2_{M_x}$ in arb. units
t in μ secs
12
14
16
18
20
22
24
26
28

TIME

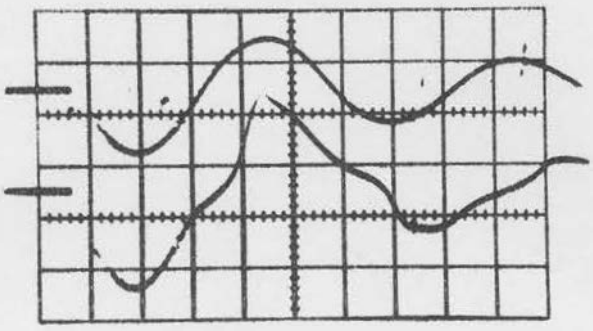

TRACE 1

Position: $-1\frac{1}{2}$, 0, $1\frac{1}{2}$

Top: Current Monitor

Bottom: B_z Vertical Scale 2100 guass/cm

Time Base: 2 μsec/cm

TRACE 2

Position: 3, 0, $4\frac{1}{2}$

Top: Current Monitor

Bottom: B_z Vertical scale 2100 guass/cm

Time Base: 2 μsec/cm

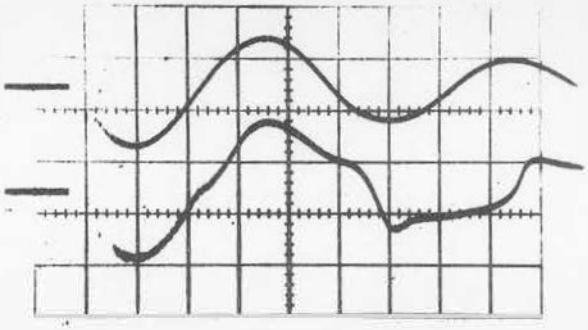

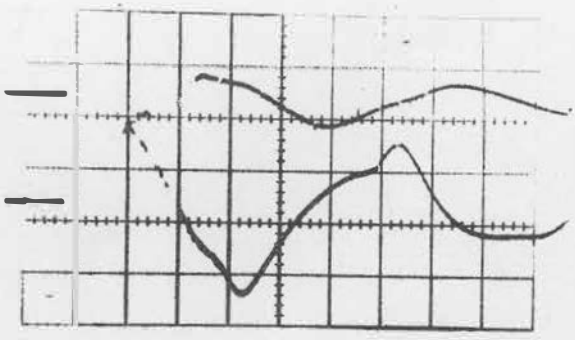

TRACE 3

Position: 3, 0, $1\frac{1}{2}$

Top: B_y Vertical Scale 1350 guass/cm

Bottom: B_x Vertical Scale 1130 gauss/cm

Time Base: 2 μsec/cm

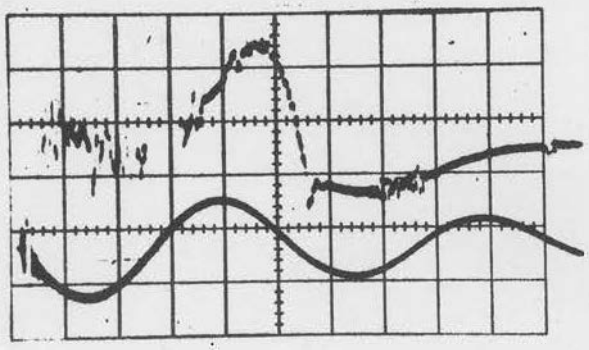

TRACE 4

Position: 6, 0, $4\frac{1}{2}$

Top: E_z Vertical Scale 17×10^3 volts/m/cm

Bottom: Current Monitor

Time Base: 2μ sec/cm

TRACE 5

Position: 0, 0, $-1\frac{1}{2}$

Top: Current Monitor

Bottom: E_z Vertical Scale 6.7×10^3 volts/m/cm

Time Base: 2μ sec/cm

Polarities reversed w.r.t. other traces

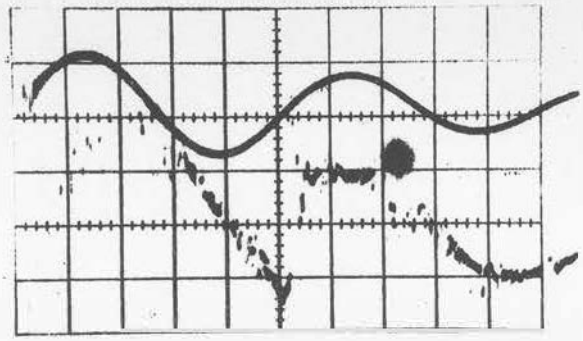

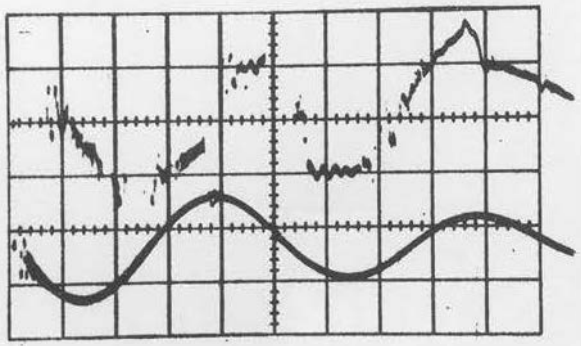

TRACE 6

Position: $-1\frac{1}{2}$, 0, 6

Top: E_z Vertical Scale 17×10^3 volts/m/cm

Bottom: Current Monitor

Time Base: 2μ sec/cm

T=22

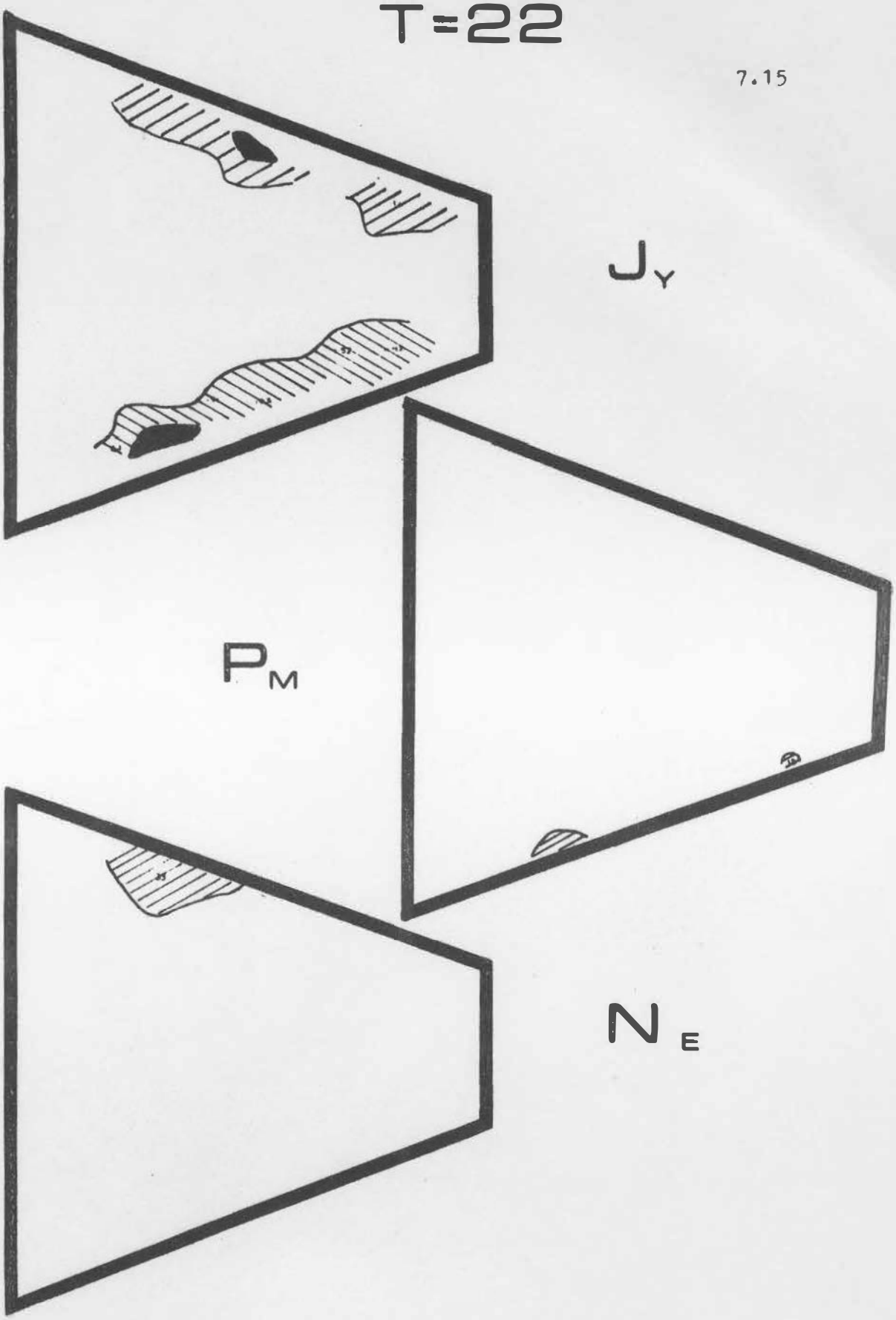

T = 23

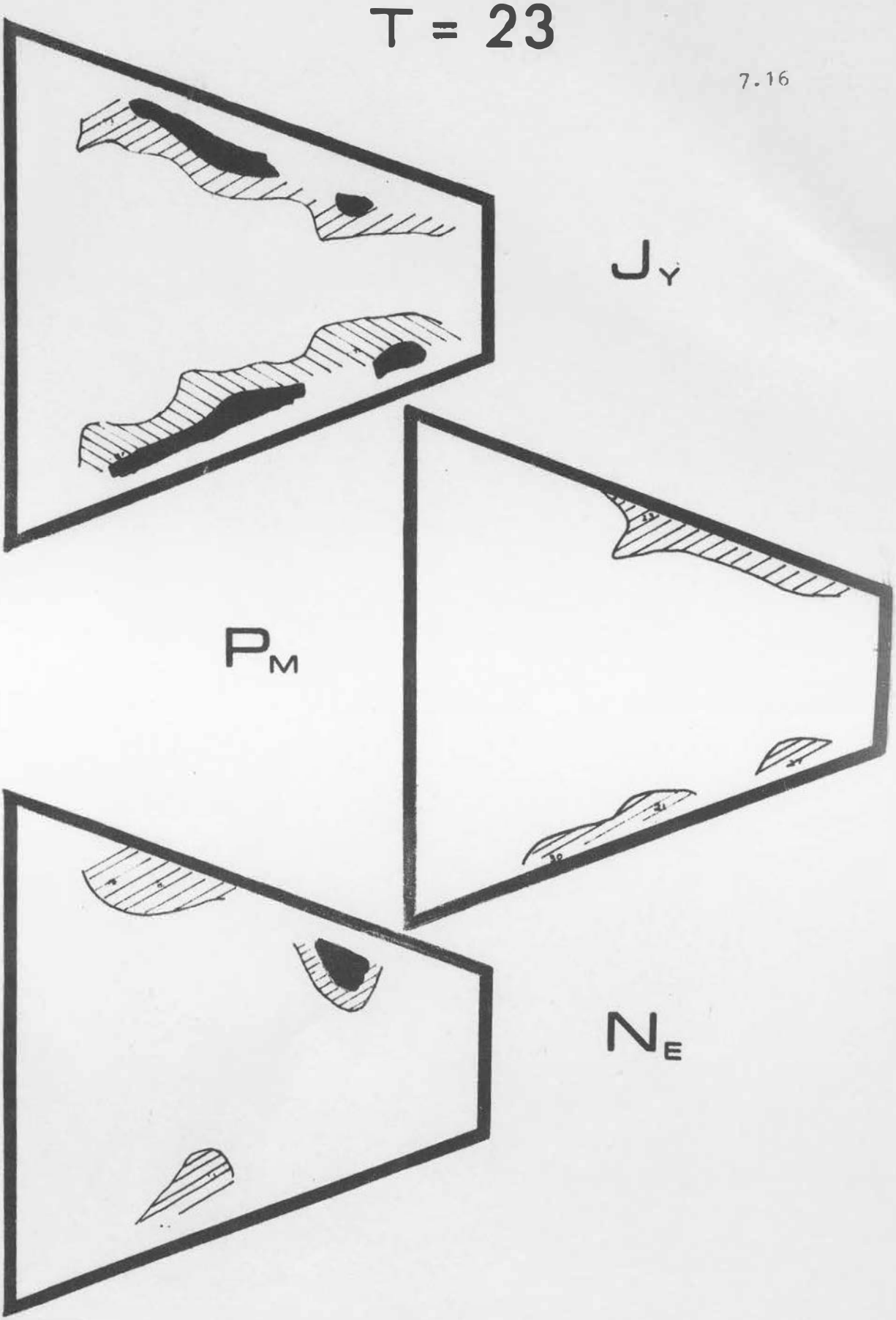

T = 24

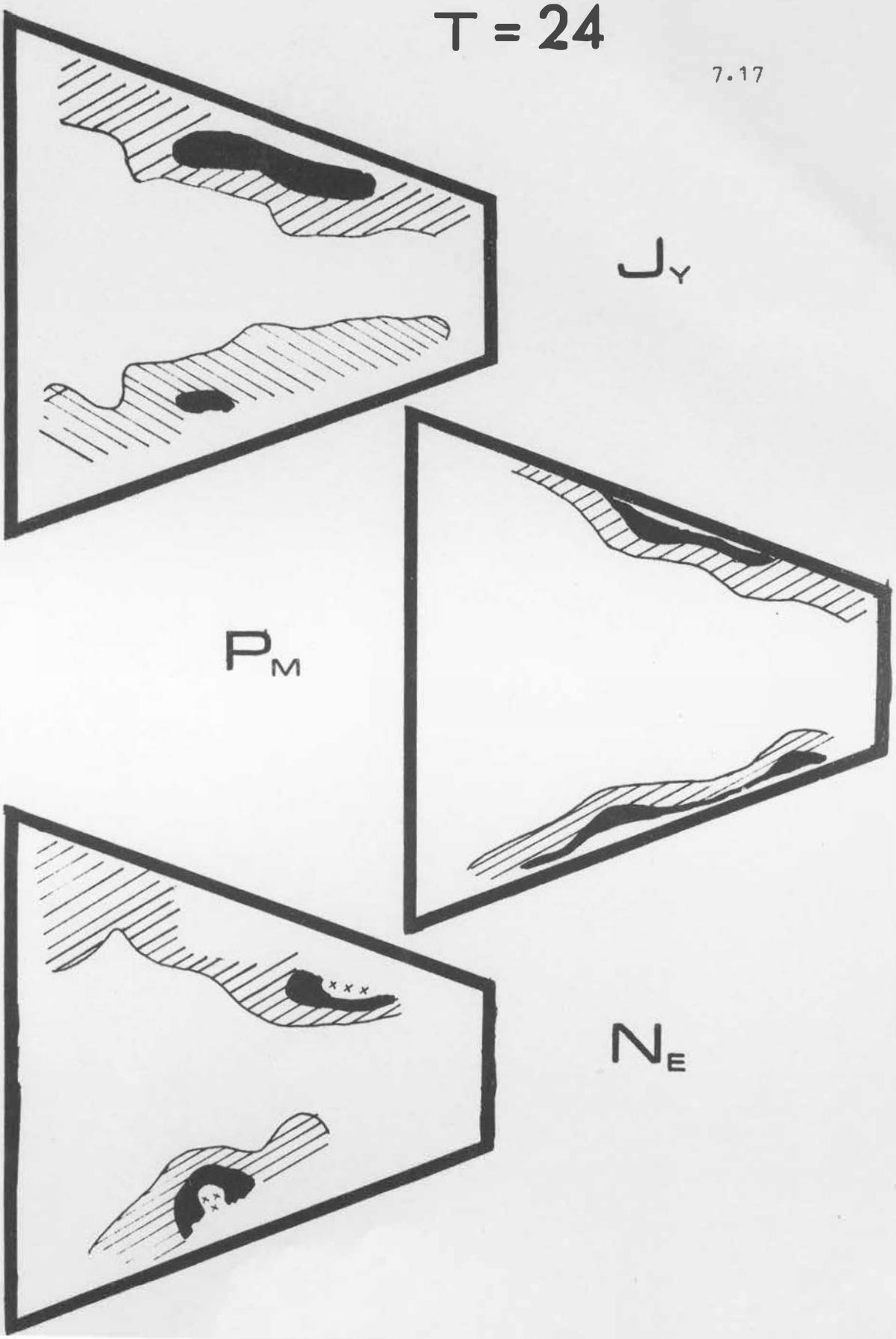

T = 25

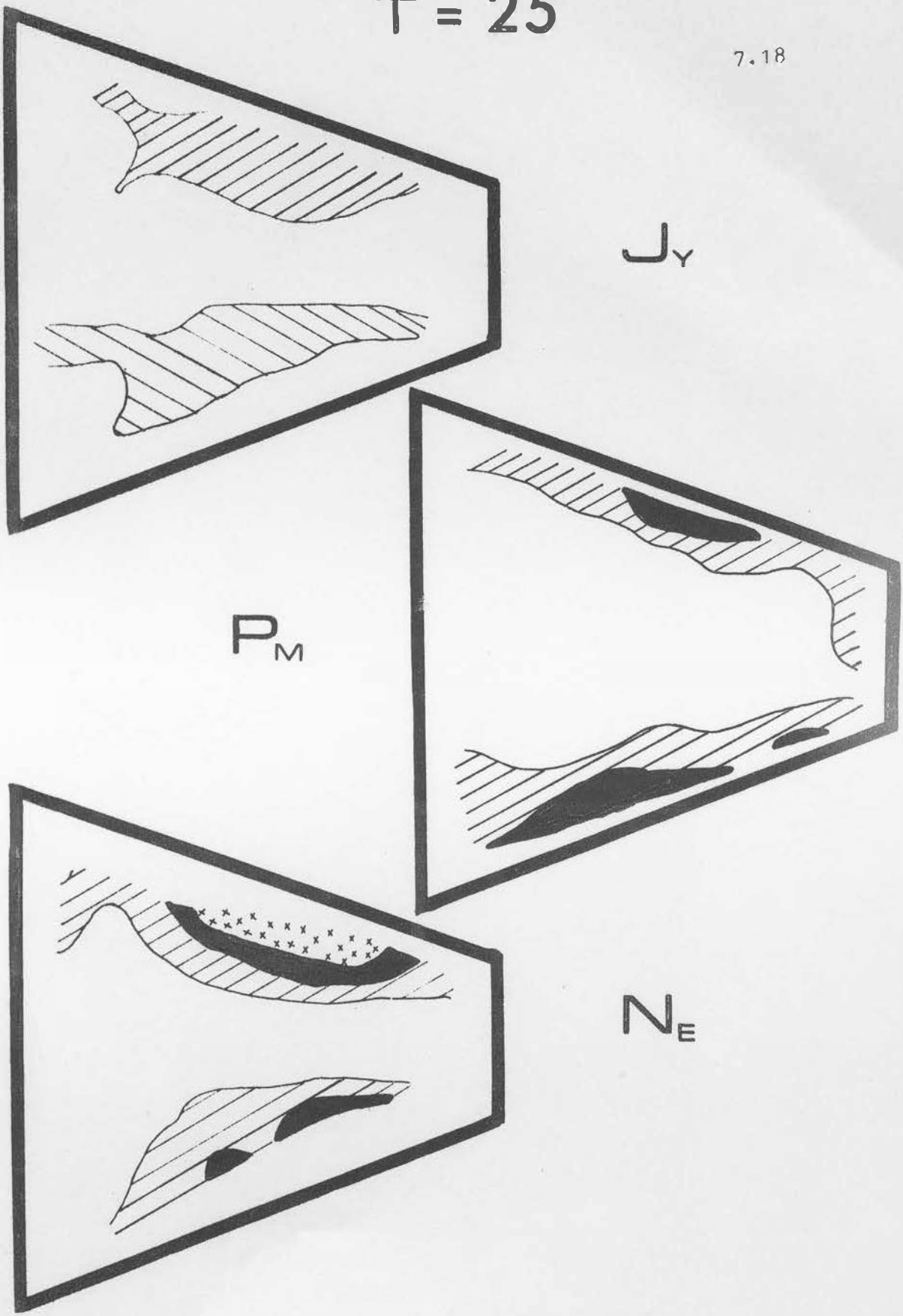

T = 26

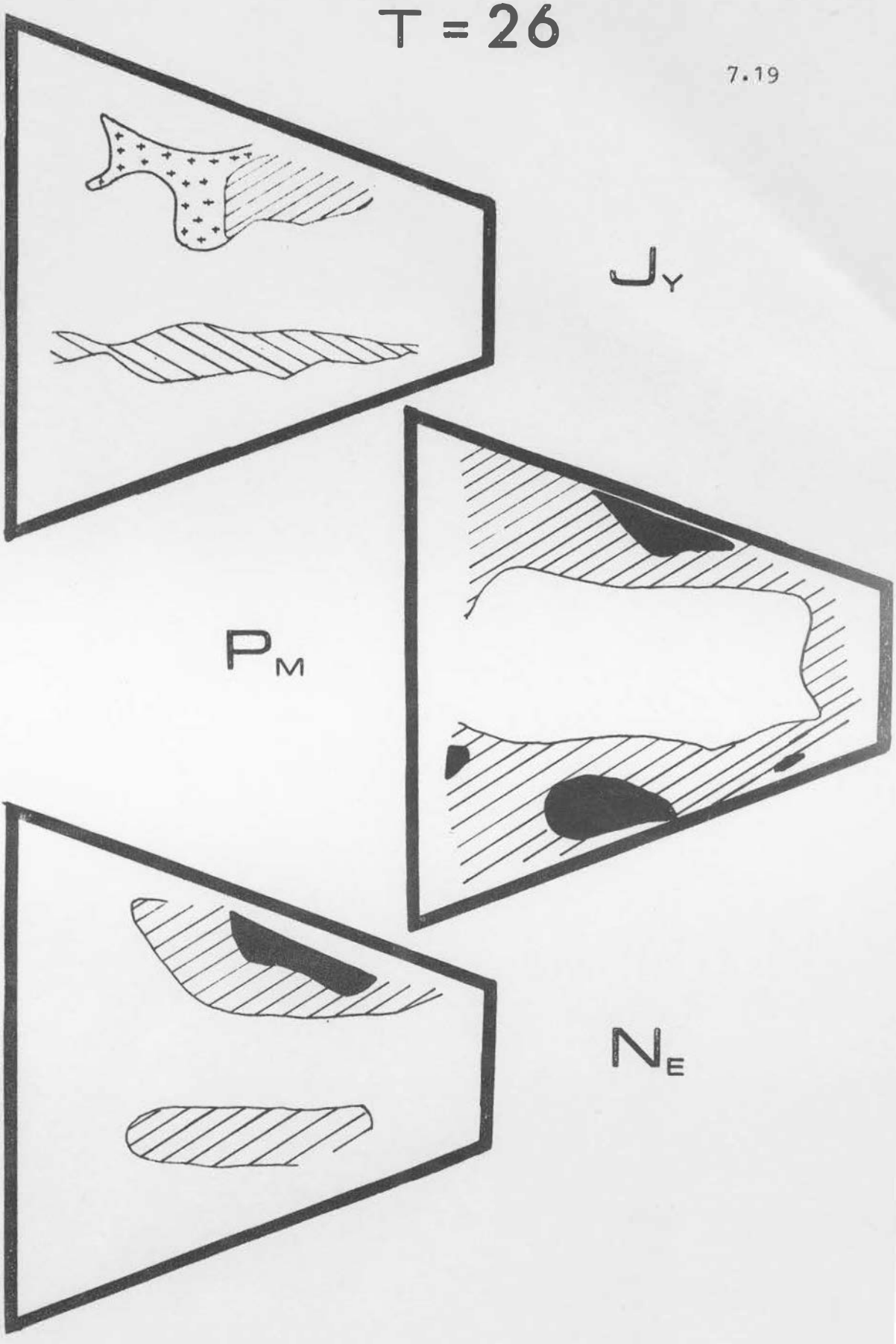

T = 27

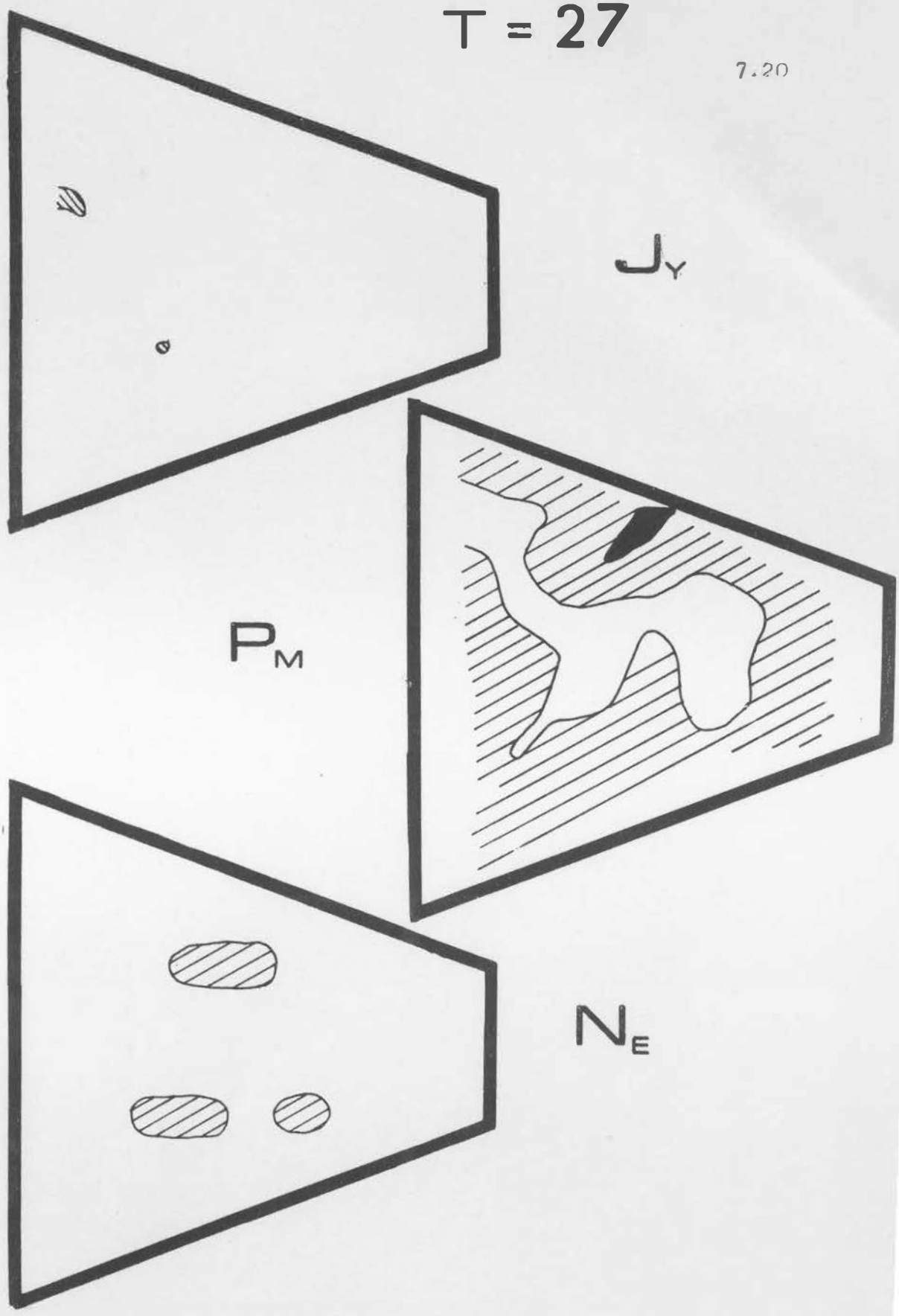

T = 28

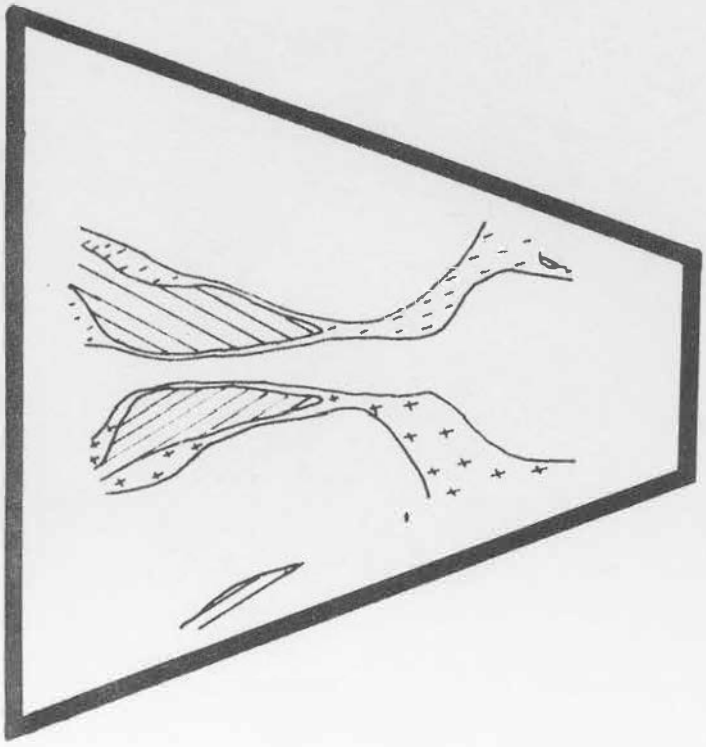

J_Y

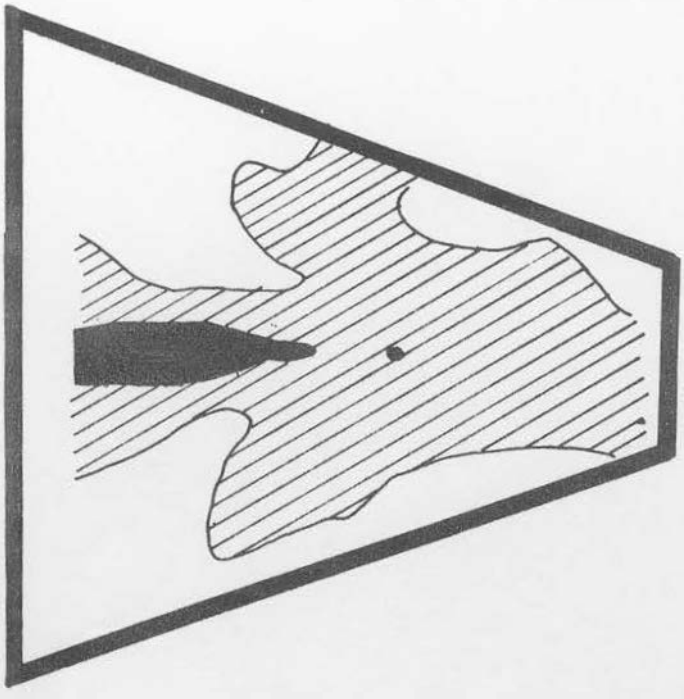

P_M

T = 29

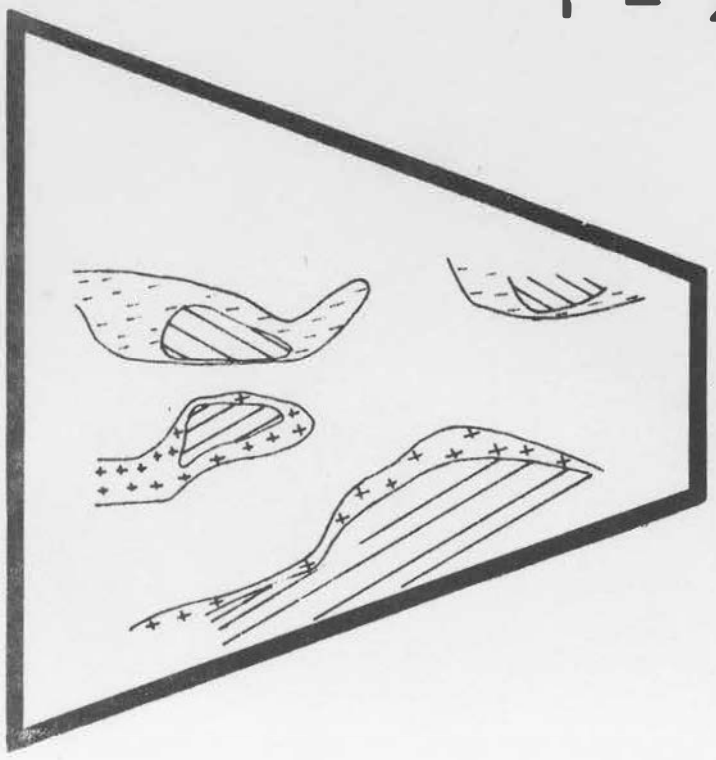

J_Y

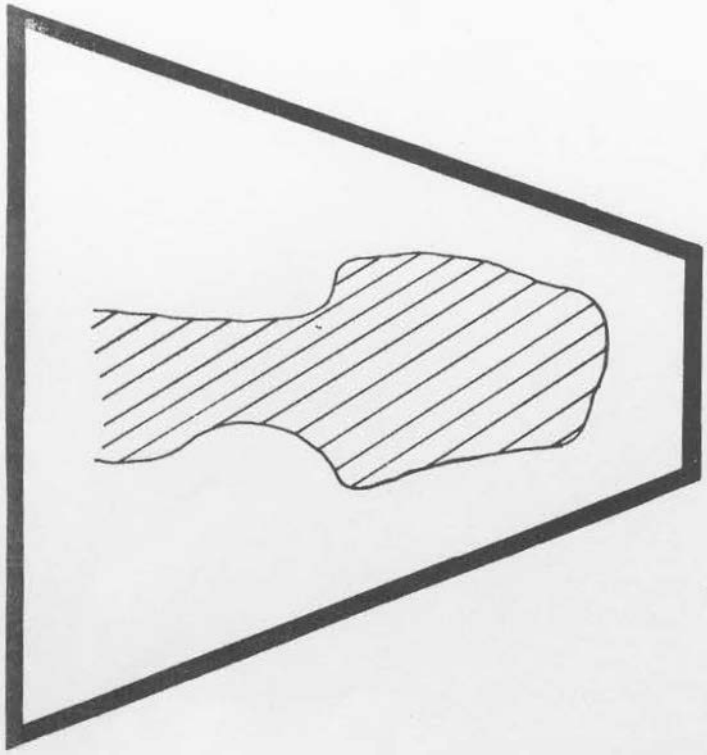

P_M

REFERENCES

(1) Burkhardt, Lovberg. Phys. Fluids 5 (341) 1962

(2) Allen, Thonemann. Proc. Phys. Soc. (London) B 67, (768) 1954

(3) J.D. Jukes. Jour. Nuc. Ener. (Part C) 6 (74) 1964

(4) N. Christofilos. Phys. Fluids 9 (1425) 1966

(5) Whiteman, McNamara, Taylor Phys. Fluids 8 (2293) 1965

(6) Grad, van Norton. Nuc. Fus. Sup. Pt I 1962

(7) Allen, Spalding. Phys. Fluids 8 (2032) 1965

(8) Berkowitz et al. Proc. Sec. U.N. Int. Conf. Peaceful Uses of At. Ener. 1958

(9) Gott, Ioffe, Telkowskii. Nucl. Fusion Sup Pt III (1045) 1962

(10) Taylor, Hastie. Phys. Fluids 8 (323) 1965

(11) eg. Rosenbluth, Krall. Phys. Fluids 8 (1004) 1965

(12) Francis, Hill, Mason Vol I Conf. Proceedings Culham 1965 (CN-21/30)

(13) F.M. Larkin. Culham Laboratory Report CLM-R37 June 1964

(14) Bernstein et al. Vol 2 Conference Proceedings Culham 1965 (CU-21/232)

(15) H. Grad. Phys. Rev. Let. 16(1147) 1966

(16) J. Andreoletti. EUR-CEA-FC-275 Oct 1964

ACKNOWLEDGEMENTS

I must thank Dr. H.S.T. Driver my tireless and ever helpful supervisor and co-experimenter, Stephanie for all the typing and her help with the diagrams, and lastly Sam for the reproduction. Some of the equipment used in the experiments was obtained from grants of the South African Council for Scientific and Industrial Research.

ERRATA

Page	Line	Read	For
1.1	9	broad	braod
2.3	15	McLeod	McCleod
4.6	5	within	with
4.8	2	theory. They	theory they
5.3	13	to avoid	avoid
5.11	3	any	as
7.2	12	a maximum	maximum